

Infection patterns in simple and complex contagion processes on networks

Diego Andrés Contreras,^{1,*} Giulia Cencetti,^{1,2,*} and Alain Barrat¹

¹*Aix-Marseille Univ, Université de Toulon, CNRS, Centre de Physique Théorique,
Turing Center for Living Systems, Marseille, France*

²*Fondazione Bruno Kessler, Trento, Italy*

Contagion processes, representing the spread of infectious diseases, information, or social behaviors, are often schematized as taking place on networks, which encode for instance the interactions between individuals. The impact of the network structure on spreading process has been widely investigated, but not the reverse question: do different processes unfolding on a given network lead to different infection patterns? How do the infection patterns depend on a model's parameters or on the nature of the contagion processes? Here we address this issue by investigating the infection patterns for a variety of models. In simple contagion processes, where contagion events involve one connection at a time, we find that the infection patterns are extremely robust across models and parameters. In complex contagion models instead, in which multiple interactions are needed for a contagion event, non-trivial dependencies on models parameters emerge, as the infection pattern depends on the interplay between pairwise and group contagions. In models involving threshold mechanisms moreover, slight parameter changes can significantly impact the spreading paths. Our results show that it is possible to study crucial features of a spread from schematized models, and inform us on the variations between spreading patterns in processes of different nature.

AUTHOR SUMMARY

Contagion processes, representing the spread of infectious diseases, information, or social behaviors, are often schematized as taking place on networks, which encode for instance the interactions between individuals. We here observe how the network is explored by the contagion process, i.e. which links are used for contagions and how frequently. The resulting infection pattern depends on the chosen infection model but surprisingly not all the parameters and models features play a role in the infection pattern. We discover for instance that in simple contagion processes, where contagion events involve one connection at a time, the infection patterns are extremely robust across models and parameters. This has consequences in the role of models in decision-making, as it implies that numerical simulations of simple contagion processes using simplified settings can bring important insights even in the case of a new emerging disease whose properties are not yet well known. In complex contagion models instead, in which multiple interactions are needed for a contagion event, non-trivial dependencies on model parameters emerge and infection pattern cannot be confused with those observed for simple contagion.

I. INTRODUCTION

Contagion processes pervade our societies. Examples include the spread of infectious diseases, both through contacts between hosts and following their mobility patterns, but also information diffusion or the propagation of social behavior [1–6]. Modeling of these processes often includes a description of the interactions among the hosts as a network, in which nodes represent individuals and a link between nodes correspond to the existence of an interaction along which the disease (or informa-

tion) can spread. In the resulting field of network epidemiology [4, 6, 7], many results have been obtained for the paradigmatic models of diffusion processes, in which the hosts can only be in a few possible states or compartments, such as susceptible (S, healthy), infectious (I, having the disease/information and able to transmit it), or recovered (R, cured and immunized) [1, 2]. These results concern mainly the context of models aimed at describing the spread of infectious diseases, represented as so-called *simple contagion* processes: namely, processes in which a single interaction between a susceptible and an infectious can lead to a transmission event [1, 6]. In this context, many studies have provided insights into how the structure of the underlying network influences the spread and impacts the epidemic threshold (separating a phase in which the epidemic dies out from one in which it impacts a relevant fraction of the population), and how various containment strategies can mitigate the spread [4, 6].

Fewer results concern the detailed analysis of the process dynamics and spreading patterns, despite its relevance [8]. In particular, the reverse question of whether different processes lead to different or similar infection patterns has barely been explored. At the population level, a robustness of the shapes of the epidemic curves has been observed for various spreading models [9, 10] and contact networks [11]. In heterogeneous networks, it has also been shown that simple contagion spreading processes first reach nodes with many neighbours, and then cascade towards nodes of smaller degree [12–14]. Moreover, in the context of metapopulation models, in which each node of the network represents a geographic area and hosts can travel between nodes on the network, possibly propagating a disease, the heterogeneity of travel patterns has been shown to determine dominant paths of possible propagation at the worldwide level [8, 15, 16], allowing for instance to provide predictions for the arrival time of a pandemic in various parts of the world [17, 18].

In addition, while these results concern simple contagion processes, it is now well known that such models

* D.A.C. and G.C. contributed equally to this work.

might not be adequate to describe some contagion mechanisms, such as social contagion of behaviors. Empirical evidence has led to the definition and study of models of *complex contagion* [3, 19]: in these models, each transmission event requires interactions with multiple infectious hosts. In particular, models involving threshold phenomena [20] or group (higher-order) interactions [21] have been put forward, but results concerning the detail of their propagation patterns are scarce [14, 22].

Overall, most results on propagation patterns concern simplified models with few compartments (such as the susceptible-infected-susceptible (SIS) and susceptible-infected-recovered (SIR)) and simple contagion processes. The question arises thus of their applicability to more realistic models and to other types of spreading processes, and of the possibility to directly apply them in concrete cases. Here we contribute to tackle these issues by investigating spreading patterns for different types of contagion models on networks and hypergraphs and by addressing the following questions: how general are the propagation patterns observed in these models, and are they similar in more realistic models with compartments including latent individuals, asymptomatic cases, etc? How well do propagation patterns of simple contagion inform us on complex contagion ones, and do the most important seeds or the nodes most easily reached differ depending on the precise model or type of contagion?

To this aim, we consider the infection network of a process [8], which gives the probability of a node to be directly infected by another one, averaged over realizations of the process, and generalize it as well to complex contagion models. We compare the resulting patterns within each model as its parameters change, between different models of simple contagion and between different types of contagion processes. We first find an extreme robustness of the contagion patterns across models of simple contagion. These patterns slightly depend on the reproductive number of the spread, but are almost completely determined by the final epidemic size. This indicates also that one can define spreader and receiver indices to quantify a node's tendency to contaminate or be contaminated by its neighbours: these indices are largely independent of the specific disease model and can thus be computed on simple cases with arbitrary parameters. The situation changes when models of complex contagion are considered. On the one hand, patterns of contagion turn out to be less robust in threshold models. On the other hand, they depend on the interplay between pairwise and group processes for models involving higher-order interactions.

II. RESULTS

A. General framework

We consider the context of network epidemiology, i.e., of spreading processes on a weighted network where nodes represent the hosts and weighted links between the hosts correspond to contacts along which a disease can spread, with probability depending on the link weight [6]. Specifically, the weighted networks we will use to

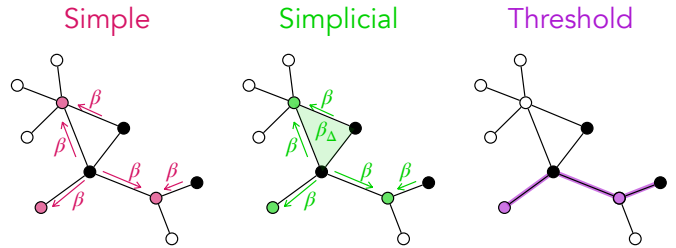


FIG. 1. **Sketch of the models of contagion considered.** In all sketches, black nodes represent infectious hosts, empty nodes are susceptible, and colored nodes represent the hosts that can be contaminated by the infectious ones. Left: Simple contagion on weighted graphs. Contagion events occur along the network edges, with probability per unit time given by β multiplied by the weight W_{ij} of the edge (i, j) between a susceptible and an infected node. Center: Simplicial model on weighted hypergraphs. Contagions can take place both along network edges (rate βW_{ij}) and if a susceptible node i is part of a group (i, j, k) with j and k both infectious (rate $\beta_{\Delta} W_{ijk}^{\Delta}$, with W_{ijk}^{Δ} the weight of the hyperedge (i, j, k)). Right: Threshold model on weighted graphs. A susceptible node becomes infected when the sum of the weights of its connections with infected nodes, divided by the total weight of its connections, exceeds a threshold θ .

perform numerical simulations of spreading processes are empirical networks obtained by temporally aggregating time-resolved data describing contacts between individuals in various contexts [23–25], where the weight W_{ij} between two individuals i and j is given by their total interaction time (see Methods).

On these networks, we will first consider several models of simple contagion, in which each node can be in several states such as susceptible, latent, infectious, and recovered, and an infectious node can transmit the infection to a susceptible neighbour with a certain probability per unit time. We will consider models with different sets of states, corresponding both to very schematic and to more realistic situations, and both Markovian and non-Markovian processes. On the other hand, we will consider a model of complex contagion that involves higher-order contagion mechanisms, i.e., interactions among groups of nodes [21]: This model describes the fact that the probability of a contagion event can be reinforced by group effects, and is defined on hypergraphs [26] in which interactions can occur not only in pairs but also in larger groups. It has indeed been shown that the inclusion of such effects leads to an important phenomenological change, with the emergence of a discontinuous epidemic transition and of critical mass phenomena. Finally, we will also consider so-called threshold models [20], in which a susceptible node becomes infected when the fraction of its interactions spent with infected neighbors reaches a threshold θ , to mimic the fact that an individual may adopt an innovation only if enough friends are already adopters. All models and their parameters are described in detail in the Methods section, and their mechanisms are sketched in Fig. 1.

For each given spreading model and propagation substrate (network or hypergraph), we perform numerical (Monte Carlo) simulations of the spread at given parameter values, starting from a single infectious seed taken at

random in the network, while all other nodes are susceptible (see Methods). The *infection pattern* of the model is then the weighted and directed graph \mathbf{C} such that C_{ij} is the probability (averaged over 1000 realizations of the spread) that node i infected node j [8, 16]. In practice, it is obtained from the numerical simulations, by counting all the direct infectious events from i towards j among all runs, and dividing by the number of runs. The infection pattern hence represents the signature of an epidemic, highlighting the paths that are taken by the contagion process with a higher probability¹. We first note that a non-zero $C_{ij} > 0$ can be obtained if and only if there exists an interaction between i and j in the weighted network; moreover, one can expect that the probability C_{ij} of i infecting j depends on the weight W_{ij} of their connection. However, it also depends on the probability of i to be infected in the first place, to be infected before j , and of j not to be infected through another interaction. Overall, one can thus expect C_{ij} to depend on non trivial properties of the network topology and not only on the weight of the link between i and j . In particular, even if the interaction weights are symmetric, this is not a priori the case for the infection pattern: the network defined by the matrix C_{ij} is directed. This is shown in Fig. 2 for a toy network, where the largest values of C_{ij} do not correspond to the largest link weights. Once \mathbf{C} is defined, we can moreover use it to compute spreader and receiver indices for each node, respectively as $s_i = \sum_j C_{ij}$ and $r_i = \sum_j C_{ji}$, i.e., as the out-strength and in-strength of each node in the directed network of the infection pattern.

It is worth noting here that \mathbf{C} , and as a consequence also the spreader and receiver indices, depend both on the specific model of spread and on its parameters. We will explore these dependencies in detail in the following sections. In this exploration, we have considered, as the support of the contagion models we investigate, data describing contacts between individuals collected in a conference [27], a hospital [28], a workplace [27], a primary school [29] and a high school [30]. The primary school contact data has been used in various studies to feed numerical simulations of infectious diseases' models [31–33] and entails rich intertwined structural and temporal features such as groups of temporarily densely connected nodes and alternating patterns of nodes being structured in groups or able to connect in a more global manner, as well as an important number of simultaneous group (higher-order) interactions [29, 34–37]. We thus show in the main text the results obtained for this data set, and we show the results for the other data sets in the supplementary material (SM).

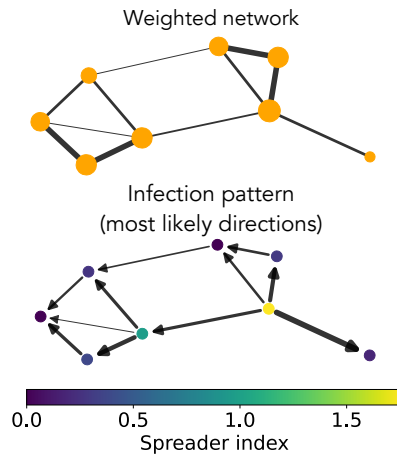


FIG. 2. **Simple contagion.** Toy network illustrating the asymmetry of the infection pattern and its dissimilarity with the adjacency matrix. The upper sketch shows the weighted adjacency matrix (links' width proportional to their weights, nodes' size proportional to their weighted degree). The lower sketch represents the infection pattern for a simple SIR contagion with $R_0 = 2$ (averaged over 500 simulations). For each connection only the direction with higher probability of infection is shown and the arrows' width is proportional to the probability. The nodes are colored according to their spreader index.

B. Simple contagion

We consider several models of simple contagion, characterized by different sets of possible states for the hosts and various types of dynamics between states. The simplest is the Susceptible-Infected-Recovered (SIR) model, in which a susceptible individual i (S) can become infected (I) with rate βW_{ij} when linked with another infected individual j by an edge of weight W_{ij} (see Fig. 1). Infected individuals then spontaneously become recovered (R) with rate μ_I and cannot participate in the dynamics anymore. The most studied extension of this model is the SEIR one, in which susceptible individuals become exposed (E, not yet contagious) with rate β upon contact with an I individual, before becoming infected. In both SIR and SEIR, we consider on the one hand fixed rates of transition from the I to the R state and from the E to the I state; the times that an individual spends in the E and I states, resp. τ_E and τ_I , are then exponentially distributed random variables (with averages given by the inverses of the transition rates). A more realistic dynamical process is obtained by a non-Markovian dynamics between these states, in which τ_E and τ_I are random variables taken from Gamma distributions with given mean and standard deviation. As both SIR and SEIR remain generic models, we also consider a more elaborate model designed to represent the propagation of COVID-19, in which individuals can be exposed and not contagious, pre-symptomatic but already infectious, infectious but asymptomatic, or infectious and symptomatic [13, 33]. These models and their parameters are described in more detail in the Methods section.

For each model and network, once the parameters of the spontaneous transitions are fixed, it is possible to

¹ C was defined for metapopulation models [8, 16] as the probability for a contagion to arrive in a geographical area from another one. Here we consider the case instead in which nodes represent hosts; moreover, this definition needs to be generalized in the case of complex contagion processes where the contagion of a node originates from several others, as described later.

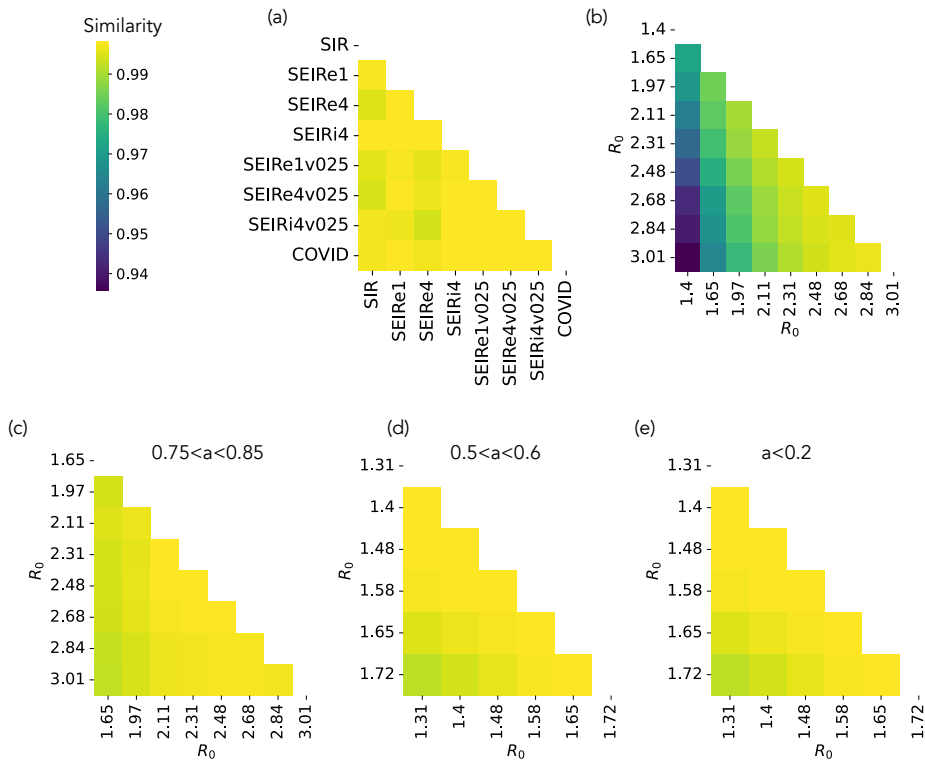


FIG. 3. Simple contagion. (a): Cosine similarity between the infection patterns of different models of simple contagion, simulated with the same $R_0 = 2.5$ (see Methods for the description of the models). (b): Cosine similarity between the infection patterns obtained at varying R_0 for the SIR model of simple contagion. (c): Cosine similarity between infection patterns at varying R_0 for the SIR model, with infection patterns computed only using runs with final attack rate between 0.75 and 0.85. (d): Same as (c) but using runs with final attack rate between 0.5 and 0.6. (e): Same as (c) but using runs with final attack rate lower than 0.2. The results in panel (c) have been obtained by comparing, for each value of R_0 , infection pattern obtained by averaging over 1000 simulations with final attack rate a in the chosen range. For panels (d) and (e) the number of simulations to average on has been increased to 10000 and 50000, respectively. Indeed, smaller values of a mean that less nodes and links are involved in each run, so that one needs to average over more runs to compute the infection probability for each link.

adjust the contagion rate β to obtain a specific value of the reproductive number R_0 , defined as the expected number of cases directly generated by one initial infected individual in a population where all other individuals are susceptible to infection [1]. For each model and parameter value, we compute the infection pattern C and the spreader and receiver indices of each node as explained above.

As expected and anticipated in the toy example of Figure 2, we find that the matrix C is asymmetric, and we show the similarity of its elements with the weighted adjacency matrix of the underlying network in the SM Section S1. We then compare in Figure 3(a) the infection patterns C obtained in different simple contagion models, calibrated so as to correspond to the same value of R_0 . The comparison is performed by computing the cosine similarity between the lists of elements of the matrices C obtained in the various cases (see Methods for the definition of cosine similarity). Even at fixed R_0 , each model entails a different time evolution of the epidemic (see SM section S2) with a different spreading velocity, and also different compartments, so corresponds to a different general process. One could hence suppose that the infection pattern could also be largely different from one model to the next. However, Figure 3(a) highlights

how the infection patterns are actually extremely similar across models, with similarity values above 0.98. Hence, the probability for each network link of being used for a contagion event is largely independent of the specific contagion model considered (at given R_0), despite the differences in their temporal evolution. In other words, contagion paths are not only stable within one model [16] but also across models. In the following analysis, we will thus focus on the simplest SIR model.

Figure 3(b) reports the cosine similarity between matrices C obtained with the SIR model at varying R_0 . Interestingly, although the similarity values are very large, they are lower than between models at fixed R_0 , revealing a weak dependency of the infection patterns on R_0 . To understand this point further, it is worth reminding that, while R_0 largely determines the initial velocity of the spread, the contagion process remains stochastic, and simulations with a fixed R_0 can lead to different final attack rates, i.e., final values of the density of recovered individuals once the spreading process is over, i.e., once no contagion can take place any longer (we show in the SM, Section S5, the resulting distributions of final attack rates for several values of R_0). We thus consider the infection patterns at different values of R_0 but at fixed final attack rate. To this aim, we need to

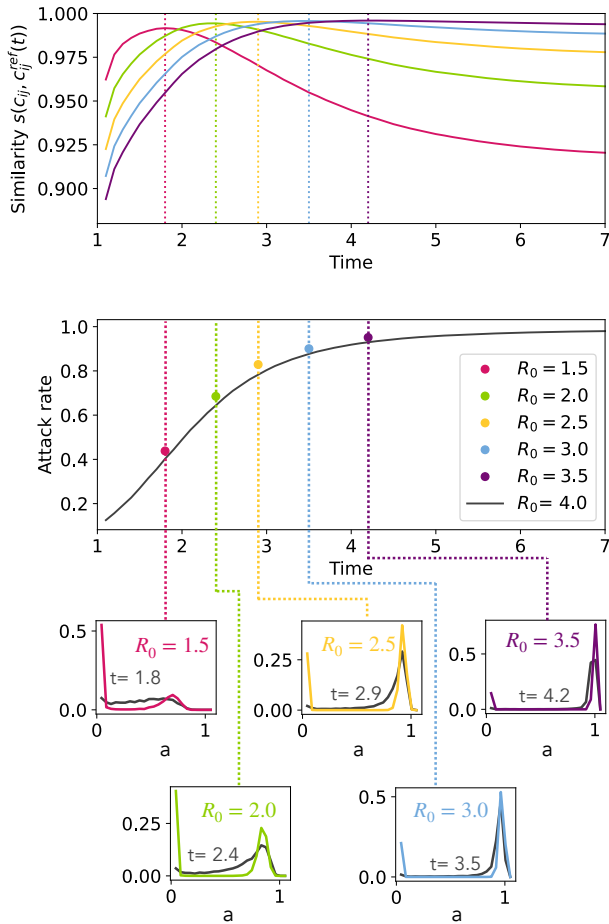


FIG. 4. **Simple contagion.** Comparison, for the SIR model, between a reference $R_0 = 4$ and five testing parameter values (R_0 from 1.5 to 3.5). Each curve in the upper panel represents the similarity in time between the temporal infection pattern $\mathbf{C}_{ref}(t)$ of the reference and the infection pattern \mathbf{C}_{R_0} of each testing parameter. $\mathbf{C}_{ref}(t)$ is computed by averaging, over 1000 numerical simulations of the SIR model at $R_0 = 4$, the contagion events occurring until t . \mathbf{C}_{R_0} is instead obtained by averaging all contagion events of 1000 numerical simulations of the SIR model at R_0 . The middle panel shows as a black curve the temporal evolution of the non-zero mode of the distributions of attack rates of the reference spread, also computed over all 1000 simulations at $R_0 = 4$ and at each time. The colored dots show, for each $R_0 \in \{1.5, 2, 2.5, 3, 3.5\}$, the value of the non-zero mode of the final attack rate distribution, computed over 1000 simulations at each R_0 . The corresponding attack rate distributions are shown in the smaller panels below.

consider compatible ranges of R_0 and final attack rates, i.e., a range of attack rates that can be reached at all the values of R_0 used. We report in Figure 3(c) the analogous of Fig. 3(b), but where the matrices \mathbf{C} have been computed taking into account only the simulations with a final attack rate between 0.75 and 0.85 (as shown in the SM, such final attack rates are reached by a non-negligible fraction of the runs for R_0 between 1.65 and 3). The similarity values become larger than 0.99, suggesting that the infection pattern of a spreading model mostly depends on its average final attack rate. To check the generality of this result, we extend this investigation

to two other ranges of final attack rates in Fig. 3(d)-(e), namely 0.5–0.6 and 0–0.2 (note that, to obtain enough simulations with final attack rates between 0.5 and 0.6, we need to consider lower values of R_0). We obtain also in these cases very high values of the similarity.

Such results moreover lead us to an additional investigation, based on two simple points: (i) the final attack rate is an increasing function of R_0 and (ii) for a given R_0 , the average attack rate is a continuously increasing function of time, which thus passes through the values of the final attack rates obtained with lower values of R_0 . The question arising is thus the following: if we consider, for a large R_0 , the time-dependent infection patterns $\mathbf{C}(t)$ (obtained by averaging on all infection events up to t), are the matrices $\mathbf{C}(t)$ similar to the final infection patterns obtained with lower values of R_0 ?

We investigate this issue in Fig. 4 through the following procedure. First, we consider as reference an SIR model with $R_0^{ref} = 4$, and perform 1000 simulations of this model. At each time, we build the time-dependent $\mathbf{C}_{ref}(t)$ by averaging on all the contagion events occurred in these 1000 simulations up to t . Second, we consider several lower values of R_0 , namely $R_0 \in \{1.5, 2, 2.5, 3, 3.5\}$, perform 1000 simulations for each value, and compute the resulting infection patterns \mathbf{C}_{R_0} . The top panel of Figure 4 displays the similarity between the time-dependent infection pattern for $R_0 = 4$, $\mathbf{C}_{ref}(t)$, and the final infection patterns obtained with the lower values of R_0 , \mathbf{C}_{R_0} . Each such similarity goes through a maximum (with large values above 0.98) as a function of time, and this maximum is obtained when the time-dependent attack rate of the reference process ($R_0 = 4$) is almost equal to the final attack rate of the process at lower R_0 , as seen in the middle panel of Fig. 4. More precisely, the 1000 simulations of the reference model yield a distribution of attack rates at each time t (displayed in black in the bottom panels of Fig. 4 for five different times). These distributions are typically bimodal and the location of the non-zero mode for each time is plotted in the middle panel of Fig. 4 (black curve). The colored dots correspond instead to the non-zero modes of the distributions of final attack rates for the lower R_0 values (full distributions shown by the colored curves in the bottom panels, obtained as well with 1000 simulations of the model for each R_0). The y-value of each coloured dot is reached by the black curve in the middle time at the same time as the maximum of the corresponding similarity curve in the top panel. Note that the similarity between $\mathbf{C}_{ref}(t)$ and \mathbf{C}_{R_0} does not reach 1 can be explained by the fact that the distributions of time-dependent and final attack rates do not coincide completely.

In other words, at each time step t of a contagion process with a high R_0 , the partial infection patterns, which describe the contagion probability of each connection until t , are extremely similar to the full infection patterns of a process with a lower value of R_0 . Vice-versa, this also means that the infection patterns of processes with low R_0 can be approximated extremely well by using a single process at large R_0 and computing its time-dependent infection patterns.

We finally also show in the SM that the range of values

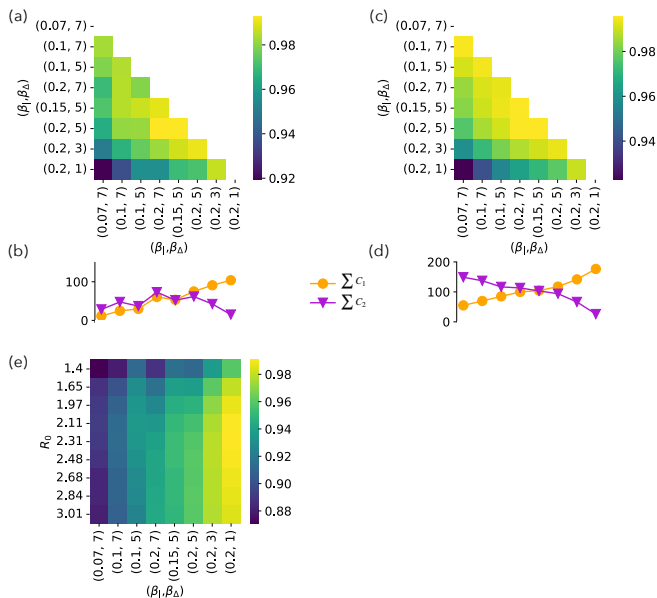


FIG. 5. **Simplicial contagion.** (a): Cosine similarity between infection patterns at varying different combinations of β_1 and β_Δ . (b): Number of contagions taking place via first and second order simplices in the simulations of the previous panel. \mathbf{C}_1 is the infection pattern matrix obtained considering only infections taking place via pairwise links and \mathbf{C}_2 is the analogous for triads infections, with $\mathbf{C}_1 + \mathbf{C}_2 = \mathbf{C}$. In the plot we report the sum of all elements of the matrices $\sum_{ij}(\mathbf{C}_1)_{ij}$ and $\sum_{ij}(\mathbf{C}_2)_{ij}$, which give the respective fractions of contagion events of each type. (c): Cosine similarity between infection patterns at varying different combinations of β and β_Δ , when computing the infection patterns using only simulations with attack rate between 0.6 and 0.7. (d): Number of contagions taking place via first and second order simplices in the simulations of the previous panel. (e): Cosine similarity between infection patterns of simplicial contagion (for the same range of values of β_1 and β_Δ) and simple contagion (for different values of R_0).

of the spreader and receiver indices depend on the reproductive number R_0 , but the ranking of nodes by these indices is very robust across models and across values of R_0 . Moreover, when fixing the attack rate, the ranges of values become equivalent even for different R_0 , and the ranking of nodes becomes almost independent of R_0 , showing that also this ranking is almost completely determined by the attack rate, and in any case very robust across parameter values. Overall, our results indicate an extreme robustness of the infection patterns across different models of simple contagion, despite their diversity in the sets of possible states for the hosts and of dynamical transition rules. Moreover, while the infection pattern does depend (very) slightly on the model parameters, it is almost completely determined by the final attack rate of the process. This result is not valid for complex contagion processes, as we will see in the next sections.

C. Simplicial contagion

Let us now consider a model of complex contagion in which the propagation can occur both on the links of the network, as in the case of simple contagion, but also on higher order (group) interactions, namely the simplicial contagion model [21], generalized here to weighted hypergraphs. As in [21], we limit ourselves for simplicity to contagion processes on first and second order interactions (pairs and triads), neglecting structures of higher orders, which will only appear as decomposed into links and triangles. We consider a SIR model, where a susceptible host i can receive the infection (i) with rate $\beta_1 W_{ij}$ when sharing a link of weight W_{ij} with an infected host j , and (ii) with rate $\beta_\Delta W_{ikl}^\Delta$ when part of a group i, k, l of three interacting nodes such that both k and l are infected (W_{ikl}^Δ being the weight of the hyperedge (i, k, l) , see Methods and Fig. 1). As in simple contagion models, infected nodes recover spontaneously - we consider here a fixed recovery rate μ_I .

As contagion events can occur both through links and triads, we here need to generalize the computation of \mathbf{C} by defining the number of infection events from i to j , $n_{i \rightarrow j}$, as follows: if j is infected by i in a pairwise interaction, $n_{i \rightarrow j}$ is incremented by one; if instead j is infected through a triadic interaction with i and l who are both infected, i and l play an equivalent role in this contagion event, and thus we divide the “responsibility” of the event equally among them: both $n_{i \rightarrow j}$ and $n_{l \rightarrow j}$ are incremented by 1/2. C_{ij} is finally the ratio of $n_{i \rightarrow j}$ to the number of numerical simulations considered.

While there is a one-to-one correspondence between R_0 and the infection rate β in the case of simple contagion (the other parameters being fixed), a given R_0 could here correspond to various pairs (β_1, β_Δ) . We thus compare the infection patterns obtained when varying both parameters in Fig. 5(a), going from a situation in which the contagion events occur mostly on triads to one in which they occur mostly on links (as shown in Fig. 5(b)). These different ratios between the two parameters β_1 and β_Δ , given they yield different relative abundances of the two types of infection (simple vs complex), can be expected to give rise to different infection patterns. The similarity values obtained remain however high, even between the most extreme cases (very different relative values of the numbers of infections in pairs and triads)². This can be explained by the observation that, in social networks, higher order interactions and pairwise ones largely overlap, i.e., nodes connected in groups with large weights are typically also connected by links with large weights (see Section S3in SM). The infection patterns on pairwise links and on triads thus also overlap. In fact, the similarity between the infection patterns of the simple SIR contagion process and the simplicial one, shown in Fig. 5(e) at varying R_0 (of

² We show in the SM results concerning the receiver and spreader indices and the subsequent ranking of nodes: similarly to the case of simple contagion, the ranking of nodes are very robust across parameter values, even if the range of values taken by the indices change.

the simple contagion) and parameters (β_1, β_Δ) , are also high, especially when the pairwise contagion events dominate in the simplicial model.

An interesting distinction with the case of simple contagion is however revealed in Fig. 5. Namely, while the infection pattern of a simple contagion process is almost completely determined when fixing its final attack rate (see Fig. 3), this is not the case for the simplicial one. We show indeed in Fig. 5(c) the similarity between infection patterns at different values of the spreading rates, but when these patterns are computed using only simulations with a given final attack rate. In contrast to the case of simple contagion, constraining the attack rate does not change the similarity values, which remain similar to the ones observed in Fig. 5(a). This is clearly due to the fact that the same attack rate can be obtained through very different relative numbers of pairwise and higher order infection events (Fig. 5(d)). The differences between simplicial contagion infection patterns at different parameters measured in Fig. 5(a) are thus mostly due to the differences in the combination between the two competing processes at work in this model (first-order vs. second-order contagions).

The simple and simplicial models entail fundamentally different contagion mechanisms, leading to different physics and different types of phase transitions, including critical mass phenomena [21, 26]. Here indeed, the differences in infection patterns are driven by the differences between pairwise and higher order contagions. However, the resulting infection patterns remain very similar in our simulations, which is probably largely due to the fact that, in the empirical data we consider, links and higher order hyperedges largely overlap, with correlated weights (see SM and [38]) so that both simple and higher order mechanisms tend to use the same infection routes. We confirm this hypothesis in the SM by showing that, if correlations between the weights of links and higher order hyperedges are removed, the similarity between the infection patterns of simple and simplicial contagion notably decreases.

D. Threshold contagion

We finally investigate the infection patterns resulting from a model of complex contagion driven by threshold effects on a network: in this model [20], a susceptible node can become infected (deterministically) only if the fraction of its neighbors that are infected overcomes a certain threshold θ , the parameter of the process (see Fig. 1). In the generalization of this model to weighted networks, a susceptible node becomes infected when the weight of its connections with infected nodes divided by the total weight of its connections exceeds the threshold. We moreover introduce a recovery parameter μ_I as in the previous cases, in order to obtain an SIR model as well. As in the simplicial model, the infection of a node i is typically due to more than one other node. We thus generalize the computation of the infection pattern \mathbf{C} similarly to the previous case: if i becomes infected because k of its neighbours i_1, i_2, \dots, i_k are infected, each $C_{i_a i}$ is incremented by $W_{i_a i} / \sum_{b=1}^k W_{i_b i}$, i.e., by the

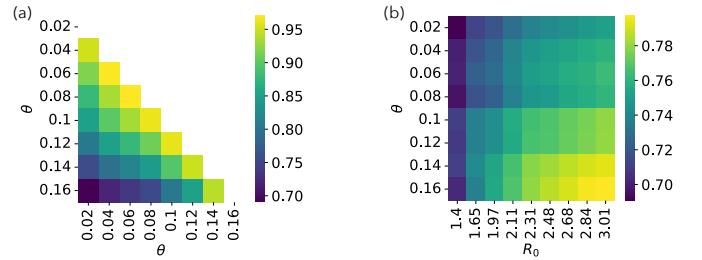


FIG. 6. **Threshold contagion.** (a): Cosine similarity between infection patterns at varying θ . (b): Cosine similarity between infection patterns of threshold contagion (for different values of θ) and simple contagion (for different values of R_0).

relative contribution of i_a to the infection event.

We compare the infection patterns of this model at various values of the parameter θ in Fig. 6(a). Interestingly, the values of the cosine similarity between patterns are still high, but typically much lower than in the previous cases, suggesting that the parameter θ plays a stronger role in determining the infection pattern than β (or R_0) in simple contagion processes (see SM for results on the receiver and spreader indices). This can be understood by the following argument: in simple contagion, all existing paths on the network can potentially support a contagion; on the other hand, changing the value of θ corresponds to allowing some infection patterns and impeding others, as it can change the number of infected neighbors needed to infect a given node. Smaller values of θ imply an easier and faster infection of nodes, while larger values only allow contagion of nodes connected with many infected, thus constraining infection to follow more specific patterns.

In Fig. 6(b) we also compare the infection patterns of the threshold contagion model with the ones of simple contagion, showing that the two processes are characterized by rather different infection patterns. The similarity is higher for larger values of θ : as θ becomes large, the condition needed for the infection of a node i becomes stricter and can be fulfilled only if the neighbours j to which i is linked by its largest weights are infected. Thus, the infection pattern becomes closer to the one of a simple process.

In general, the infection patterns for the threshold model show a higher parameter dependency with respect to the simple models. However, the values of the similarities between infection patterns obtained in Fig. 6 remain rather high, typically above 0.7. This is due to the fact that in all cases the infection patterns largely depend on (and are correlated with) the underlying weighted adjacency matrix (see SM Section S1).

III. DISCUSSION

We have here investigated the infection patterns of various models of contagion processes on networks, using as substrate several empirical networks of contacts between individuals. In particular, while it is well known that the network structure impacts the spreading pat-

terns, the question of how these patterns depend on the type of model considered (e.g., schematic or more realistic set of compartments, Markovian dynamics or more realistic transitions), on a model’s parameters, or on the type of spreading process considered (i.e., simple vs. complex contagion) has been much less considered. Understanding these issues has however important consequences in the articulation between modeling and decision making, as modeling and theoretical investigations often focus on simple models with arbitrary parameters, while one could argue that decision making should be based on models as realistic as possible. Here, we have shed light on these questions by investigating the infection patterns, defined as measuring for each connected pair of nodes of the network the probability that an infection event occurs from one to the other [8, 16].

We have obtained results along four main directions. First, we have shown that these patterns are extremely robust in models of simple contagion. This robustness is in agreement with previous results obtained each within one specific model, such as the existence of a pattern of cascading dynamics from hubs towards less connected nodes in paradigmatic models of spread [12, 13, 39], or the possibility to define epidemic pathways making the spreading pattern of a disease on a network quite predictable [8, 15, 16]. These results also rationalize the fact that arrival times of a disease spread on a network can be obtained from purely topological measures [17]. We here extend however significantly previous literature by generalizing the robustness across a large ensemble of possible models typically used to describe the evolution of infectious diseases, even if they differ in the compartments used, in the parameters and, as a result, in the resulting dynamics timescales. In particular, within one model the spreading patterns slightly depend on the reproductive number but are almost fully determined by the final attack rate.

Second, the infection patterns also allow us to define a receiver and a spreader indices for each node, which give a ranking of nodes according to their relative risk of becoming infected during the spread and to spread to other nodes. The corresponding ranking of nodes is also very robust across models and parameters. Interestingly, this result gives support to, and puts on a firmer ground, a wealth of previous literature using topological centrality measures to predict epidemic sizes or to determine which nodes would be the best “sentinels” (i.e., nodes easily reached by a disease and hence to monitor more closely in a surveillance program). Most such studies indeed use very simple spreading models with often arbitrary parameters [40–44], and our results explain why correlations between a topological centrality and measures of epidemic impact are robust against parameter changes [45], making it indeed possible to limit such studies to a restricted set of models and parameters.

Third, we have generalized the infection patterns to complex contagion processes (typically used to describe social contagion) in which each contagion event can involve several infecting nodes. We have observed that the infection patterns are then less robust; in models where simple and complex contagion events can co-exist, the robustness of patterns and their similarity to the

case of simple processes depends on the ratio between events of simple and complex contagions. In a threshold-based model, patterns differ more across parameter values. Fourth, the similarity between the averaged infection patterns discussed here remains in all cases rather high, even between contagion processes of different nature. Both these results concerning complex contagion spreading patterns constitute a major new contribution to the literature, as we are aware of almost no result on this topic. Notably, the observed high similarity might at first glance seem to contradict a previous contribution, which showed that observing the propagation patterns of single processes makes it possible to distinguish between processes based on simple contagion, higher-order contagion, or threshold processes [14]. However, we consider here averages, which are indeed all correlated with the matrix of link weights describing the network, while [14] considered individual single realizations; moreover, the fact that spreading patterns are similar does not mean that they are indistinguishable, and indeed the results of [14] relied on machine learning techniques trained on a well-chosen set of features to manage to perform the distinction between different types of processes.

Our results have interesting implications that can impact our way of thinking about and performing numerical simulations of spreading processes for decision-making purposes. First, the extreme robustness of the spreading patterns for models of simple contagion implies that simulations of very schematic models with arbitrary parameters carry an enormous amount of information on the dynamics of spreading processes with apparently much more complicated dynamics. It is also possible to use these schematic models to provide a ranking of the risk of nodes to be reached, or of their spreading power: this ranking will indeed remain remarkably accurate for different processes. This is very important as, when a new disease emerges, it is initially difficult to estimate its parameters and sometimes even the types of compartments that should be taken into account in its modeling. Even in such cases, simulations with simplified models can thus bring interesting initial insights.

Second, even if single instances of simple and complex contagion processes present differences [14], it is also noteworthy that, when considering average infection patterns, their similarity remains high. Schematic simple contagion models can thus still be used to obtain information on the patterns of a social contagion process, and on the ranking of hosts in terms of their probability to be reached or their ability to propagate. However, the uncertainty on such ranking is higher than with simple contagion processes if the precise mechanism determining the propagation (e.g., depending on a threshold, or implying group effects) and the corresponding parameters are unknown.

Third, the stronger dependency of complex contagion processes on models and parameters implies the need for additional tools to determine whether an observed contagion process is determined by simple or complex contagion mechanisms. A first step in this direction was performed in [14], but more investigations, especially on real (social) contagion data, are desirable. Moreover, as the infection patterns depend on the ratio of con-

tagion events occurring in pairwise events or in larger group, data collection efforts should explicitly target the measure of group interactions and not be restricted to pairwise representations of the system under scrutiny, in order to correctly inform models.

Our work has limitations worth mentioning, which also open some avenues for future work. The set of networks on which we have performed our investigation corresponds to diverse contexts of empirical contacts and thus entails a variety of complex interaction patterns, but remains limited. It would be interesting to extend our study to synthetic (hyper)networks where the distributions of degrees and of group sizes and the overlap between dyads and triads could be controlled. Our work also deals with static networks, and could be extended to temporal networks, especially as the propagation paths and infection risk might then be measured during a certain period while the propagation could then take place at another time [46, 47]. Finally, the infection patterns could also be studied for other models of complex contagion (including contagion events in groups of arbitrary sizes [48]).

IV. METHODS

A. Models of simple contagion

We consider three different epidemic processes, all of them agent-based compartmental models, i.e., in which each agent (represented by a node of the network) can pass through a finite set of possible compartments describing the evolution of a disease.

In the SIR model, a susceptible node i (in compartment S) can become infected (changing compartment to I) by contact with one of its neighbors on the network j . This transition takes place with rate βW_{ij} , where β is the infection rate, a free parameter of the model, and W_{ij} is the weight of the connection between i and j . Each node will then recover (becoming R) independently at rate μ_I , another free parameter. We note that, as we consider processes occurring on static networks, rescaling all parameters by the same factor does not change the dynamics but only sets a global time scale. We thus consider for simplicity parameters of order 1 in all cases.

The SEIR model is similar to the previous one with the addition of one state: exposed (E). Newly infected individuals first enter the exposed (non-infectious) state and, with a rate μ_E , they transition to the infectious state. Again, they will recover at rate μ_I . We consider three versions of SEIR models: SEIRe1, SEIRe4, and SEIRi4, which only differ by the values of their parameters, which are given in Table I. SEIRe1 is a baseline in which all rates are equal, and in each variation we change one of the parameters by a factor 4, making the average duration of the corresponding state four times longer (for instance in SEIRe4, a node spends on average four times more time in the exposed state than in the SEIRe1 version), so that these average durations differ significantly in the different models, but do not change order of magnitude (which would be unrealistic).

In both SIR and SEIR, the recovery rate μ_I and the

exposed-to-infected rate μ_E are constant, implying that the times spent by an agent in the infected and exposed states are random variables drawn from exponential distributions with respective averages $\tau_I = 1/\mu_I$ and $\tau_E = 1/\mu_E$ (which are thus gamma distributions with standard deviations $\sigma_X = \tau_X$ with $X = I, E$). Instead of constant rates, we can also consider times in the E and I states distributed according to gamma distributions with averages $\tau_E = 1/\mu_E$ and $\tau_I = 1/\mu_I$ and standard deviations $\sigma_X = \eta_X \tau_X$ with $\eta \neq 1$, thus obtaining non-markovian models. We consider the extension of the three versions of the SEIR model (SEIRe1, SEIRe4, and SEIRi4) to this non-markovian framework, namely SEIRe1v025, SEIRe4v025, and SEIRi4v025. In these models, the average durations τ_I and τ_E are the same as in the Markovian versions, but the standard deviations are reduced by a factor 4 with respect to the Markovian cases: this yields clearly different distribution of the durations of the states with respect to the Markovian case, without going to extreme, unrealistic cases (see Table I).

We also consider the COVID model describing the propagation of SARS-CoV2 used in [13, 33]. In this model, when a susceptible agent is contaminated it transitions to an exposed state followed by a pre-symptomatic infectious state, remaining in these states for times extracted from gamma distributions with respective averages τ_E and τ_p , and standard deviations σ_E and σ_p . Then individuals can either evolve into a sub-clinical infection or manifest a clinical infection, with respective probabilities $1 - p_c$ and p_c . The duration in the infectious state is extracted from a gamma distribution with average τ_I and standard deviation σ_I . An individual i in the infected states (pre-symptomatic, sub-clinical or clinical) can transmit the disease to a susceptible individual j when in contact with it with respective rates of transmission $r_p \beta W_{ij}$, $r_{sc} \beta W_{ij}$, and βW_{ij} . We use here the same parameter values as in [13, 33].

Table I shows the values for the different parameters used in these models. Moreover, in all cases, the parameter β is tuned to obtain a desired specific value for the basic reproductive number R_0 , as detailed in the next section.

B. Reproductive number and calibration of the simple contagion models

The reproductive number, R_0 , is defined as the average number of cases directly generated by one infected individual in a population where all the others are susceptible. In detail, each simulation begins with one random infected node i and we count all the neighbors of i that are directly infected by it until i becomes recovered, obtaining a potentially different value in each stochastic simulation. Averaging over these values at fixed parameters yields R_0 .

Specifically, we perform 1000 simulations for 20 values of β to obtain the corresponding values of R_0 (ranging between 1 and 4) and thus a correspondence table between β and R_0 . For each desired value of R_0 , it is then enough to interpolate between the values in the table to obtain the value of β needed in the simulations.

TABLE I. Simple contagion model parameters.

SIR model	μ_I					
SIR	0.25					
Markovian						
SEIR models	μ_E	η_E	μ_I	η_I		
SEIRe1	1	1	1	1		
SEIRe4	0.25	1	1	1		
SEIRi4	1	1	0.25	1		
Non-Markovian						
SEIR models	μ_E	η_E	μ_I	η_I		
SEIRe1v025	1	0.25	1	0.25		
SEIRe4v025	0.25	0.25	1	0.25		
SEIRi4v025	1	0.25	0.25	0.25		
COVID						
model	$\tau_E \pm \sigma_E$	$\tau_p \pm \sigma_p$	$\tau_I \pm \sigma_I$	p_c	r_p	r_{sc}
COVID	4 ± 2.3	1.8 ± 1.8	5 ± 2.0	0.5	0.55	0.55

C. Data sets

We use high-resolution face-to-face empirical contacts data collected using wearable sensors in different settings. The data sets are publicly available on the website <http://www.sociopatterns.org/datasets>. Data sets are available as lists of contacts over time (with a temporal resolution of 20 s) between anonymized individuals. The considered data sets are:

- **Primary school**, which describes the contacts among 232 children and 10 teachers in a primary school in Lyon, France, during two days of school activity in 2009 [49]. The school is composed of 5 grades, each of them comprising 2 classes, for a total of 10 classes.
- **Workplace**, gathering the contacts among 214 individuals, measured in an office building in France during two weeks in 2015 [27].
- **Hospital**, which describes the interaction among 42 health care workers (HCWs) and 29 patients in a hospital ward in Lyon, France, gathered during three days in 2010 [50].
- **High school**, describing the contacts among 324 students of "classes préparatoires" in Marseille, France, during one week in 2013 [51].
- **Conference**, which describes the interactions of 405 participants to the 2009 SFHH conference in Nice, France [52].

D. From the data to weighted graphs and hypergraphs

As explained in the previous section, the data sets we use describe temporally resolved interactions between

individuals. Each data set is provided as a list of interactions between individuals. Each element of the list corresponds to a time in which two individuals were registered as in interaction. Each such interaction event is reported in the form " $t \ i \ j$ " where t indicates the time, with a temporal resolution of 20 seconds, and i and j the involved individuals identification numbers.

For each data set we obtain a weighted static network by aggregating over time as follows:

- each individual involved in the data collection is represented by a node of the network;
- each pair of nodes (i, j) appearing in the list of events is represented as a link ij between nodes i and j in the network;
- we denote by n_{ij} the number of times that the pair (i, j) appears in the data set (the total contact duration between the corresponding individuals is thus n_{ij} times 20 seconds);
- we compute the maximum of these numbers over all pairs of individuals, $n_{max} = \max_{i,j} n_{ij}$;
- the weight of the link ij is given by n_{ij}/n_{max} .

We then use the weighted networks resulting from this procedure to simulate the spreading models of simple and threshold contagion, in which contagion events involve only links.

We moreover use the data sets to build weighted hypergraphs involving both links (hyperedges of size 2, or "first-order interactions") and hyperedges of size 3 (so-called "second-order interactions", i.e., interactions between 3 nodes). We build the hypergraphs as in [21]. Namely, we first consider all the links of the weighted graphs obtained as above: these links form the weighted hyperedges of size 2 of the hypergraph. To build the second-order interactions, we first identify all the simultaneous interactions at each time t , obtaining so-called "snapshot graphs": the snapshot graph at time t is simply the network of all interactions taking place at t . In each snapshot graph, we identify its cliques (sets of nodes all interacting with each other) of size at least 3. For instance, if at t the interactions (i, j) , (i, k) , (j, k) are present, then ijk is a clique at time t . If a clique of size larger than 3 is present, such as $ijkl$, we decompose it into all the possible triads, here ijk , ijl , ikl , jkl . We then proceed as for the weighted graphs, namely

- each triad ijk appearing at least in one snapshot becomes a hyperedge of size 3 of the weighted hypergraph;
- we denote by n_{ijk} the number of snapshots in which the triad ijk appears;
- we compute the maximum of these numbers over all triads of individuals, $n_{max}^{(2)} = \max_{i,j,k} n_{ijk}$;
- the weight of the hyperedge ijk is given by $n_{ijk}/n_{max}^{(2)}$.

We use the resulting weighted hypergraphs in the numerical simulations of the simplicial contagion processes.

E. Cosine similarity

The cosine similarity $cs(v, w)$ quantifies the similarity between two vectors \mathbf{v} and \mathbf{w} of the same dimension n . It is defined as:

$$cs(\mathbf{v}, \mathbf{w}) = \frac{\mathbf{v} \cdot \mathbf{w}}{\|\mathbf{v}\| \|\mathbf{w}\|} = \frac{\sum_{i=1}^n v_i w_i}{\sqrt{\sum_{i=1}^n v_i^2} \sqrt{\sum_{i=1}^n w_i^2}}. \quad (1)$$

It is bounded in $[-1, 1]$. It is equal to 1 when one vector is proportional to the other with a positive proportionality factor, and to 0 if they are orthogonal.

In order to measure the similarity between two infection patterns we generate two vectors from the corresponding C matrices (concatenating all the rows of one matrix) and we apply the definition of cosine similarity to the two resulting vectors. Since all the elements of C are non-negative, the cosine similarity is here bounded in $[0, 1]$.

V. CODE AVAILABILITY

The code used for numerical simulations and analyses of infection patterns is publicly available at the following link: https://github.com/giuliacencetti/Infection_pattern

ACKNOWLEDGMENTS

This work was supported by the Agence Nationale de la Recherche (ANR) project DATAREDUX (ANR-19-CE46-0008). G.C. acknowledges the support of the European Union's Horizon 2020 research and innovation program under the Marie Skłodowska-Curie grant agreement No 101103026. The funders had no role in study design, data collection and analysis, decision to publish, or preparation of the manuscript.

-
- [1] Anderson RM, May RM. *Infectious Diseases of Humans: Dynamics and Control*. Oxford: Oxford University Press; 1992.
 - [2] Keeling MJ, Rohani P. *Modeling infectious diseases in humans and animals*. Princeton University Press; 2011.
 - [3] Centola D, Macy MW. Complex Contagions and the Weakness of Long Ties. *American Journal of Sociology*. 2007;113(3):702-34. Available from: <https://doi.org/10.1086/521848>.
 - [4] Barrat A, Barthelemy M, Vespignani A. *Dynamical Processes on Complex Networks*. Leiden: Cambridge University Press; 2008.
 - [5] Castellano C, Fortunato S, Loreto V. Statistical physics of social dynamics. *Rev Mod Phys*. 2009 May;81:591-646. Available from: <https://link.aps.org/doi/10.1103/RevModPhys.81.591>.
 - [6] Pastor-Satorras R, Castellano C, Van Mieghem P, Vespignani A. Epidemic processes in complex networks. *Rev Mod Phys*. 2015 Aug;87:925-79. Available from: <https://link.aps.org/doi/10.1103/RevModPhys.87.925>.
 - [7] Pastor-Satorras R, Vespignani A. Epidemic dynamics and endemic states in complex networks. *Physical Review E*. 2001;63(6):066117.
 - [8] Piontti APY, Gomes MFDC, Samay N, Perra N, Vespignani A. The infection tree of global epidemics. *Network Science*. 2014;2(1):132-7.
 - [9] Heng K, Althaus CL. The approximately universal shapes of epidemic curves in the Susceptible-Exposed-Infectious-Recovered (SEIR) model. *Scientific Reports*. 2020;10(1):1-6.
 - [10] Keliger D. Universality of SIS epidemics starting from small initial conditions. arXiv preprint arXiv:220402092. 2022.
 - [11] Bioglio L, Génois M, Vestergaard CL, Poletto C, Barrat A, Colizza V. Recalibrating disease parameters for increasing realism in modeling epidemics in closed settings. *BMC Infectious Diseases*. 2016;16(1):1-15. Available from: <http://dx.doi.org/10.1186/s12879-016-2003-3>.
 - [12] Barthélemy M, Barrat A, Pastor-Satorras R, Vespignani A. Dynamical patterns of epidemic outbreaks in complex heterogeneous networks. *Journal of theoretical biology*. 2005;235(2):275-88.
 - [13] Contreras DA, Colosi E, Bassignana G, Colizza V, Barrat A. Impact of contact data resolution on the evaluation of interventions in mathematical models of infectious diseases. *J R Soc Interface*. 2022;19:20220164.
 - [14] Cencetti G, Contreras DA, Mancastroppa M, Barrat A. Distinguishing Simple and Complex Contagion Processes on Networks. *Phys Rev Lett*. 2023 Jun;130:247401. Available from: <https://link.aps.org/doi/10.1103/PhysRevLett.130.247401>.
 - [15] Colizza V, Barrat A, Barthelemy M, Vespignani A. The role of the airline transportation network in the prediction and predictability of global epidemics. *Proc Natl Acad Sci USA*. 2006;103:2015-20.
 - [16] Colizza V, Barrat A, Barthelemy M, Vespignani A. Predictability and epidemic pathways in global outbreaks of infectious diseases: the SARS case study. *BMC Medicine*. 2007;5:34.
 - [17] Gautreau A, Barrat A, Barthelemy M. Global disease spread: Statistic and estimation on arrival times. *J Theor Biol*. 2008;251:509-22.
 - [18] Tizzoni M, Bajardi P, Poletto C, Ramasco JJ, Balcan D, Gonçalves B, et al. Real-time numerical forecast of global epidemic spreading: case study of 2009 A/H1N1pdm. *BMC Medicine*. 2012;10:165.
 - [19] Centola D. The spread of behavior in an online social network experiment. *Science*. 2010;329(5996):1194-7.
 - [20] Watts DJ. A simple model of global cascades on random networks. *Proceedings of the National Academy of Sciences*. 2002;99(9):5766-71.
 - [21] Iacopini I, Petri G, Barrat A, Latora V. Simplicial models of social contagion. *Nature communications*. 2019;10(1):2485.
 - [22] Hébert-Dufresne L, Scarpino SV, Young JG. Macroscopic patterns of interacting contagions are indistinguishable from social reinforcement. *Nature Physics*. 2020;16(4):426-31.
 - [23] SocioPatterns collaboration; 2008. Accessed: 2022-11-25. <http://www.sociopatterns.org/>.
 - [24] Cattuto C, Van den Broeck W, Barrat A, Colizza V, Pinton JF, Vespignani A. Dynamics of Person-to-Person Interactions from Distributed RFID Sensor Networks. *PLoS ONE*. 2010 07;5(7):e11596.

- [25] Barrat A, Cattuto C. In: Gonçalves B, Perra N, editors. *Face-to-Face Interactions*. Cham: Springer International Publishing; 2015. p. 37-57. Available from: https://doi.org/10.1007/978-3-319-14011-7_3.
- [26] Battiston F, Cencetti G, Iacopini I, Latora V, Lucas M, Patania A, et al. Networks beyond pairwise interactions: structure and dynamics. *Physics Reports*. 2020;874:1-92.
- [27] Géniois M, Barrat A. Can co-location be used as a proxy for face-to-face contacts? *EPJ Data Science*. 2018 May;7(1):11. Available from: <https://doi.org/10.1140/epjds/s13688-018-0140-1>.
- [28] Vanhems P, Barrat A, Cattuto C, Pinton JF, Khanafer N, Régis C, et al. Estimating Potential Infection Transmission Routes in Hospital Wards Using Wearable Proximity Sensors. *PLoS ONE*. 2013 09;8(9):e73970.
- [29] Stehlé J, Voirin N, Barrat A, Cattuto C, Isella L, Pinton J, et al. High-Resolution Measurements of Face-to-Face Contact Patterns in a Primary School. *PLoS ONE*. 2011 08;6(8):e23176. Available from: <http://dx.doi.org/10.1371/journal.pone.0023176>.
- [30] Mastrandrea R, Fournet J, Barrat A. Contact patterns in a high school: a comparison between data collected using wearable sensors, contact diaries and friendship surveys. *PLoS one*. 2015;10(9):e0136497.
- [31] Gemmetto V, Barrat A, Cattuto C. Mitigation of infectious disease at school: targeted class closure vs school closure. *BMC infectious diseases*. 2014 Dec;14(1):695.
- [32] Ciavarella C, Fumanelli L, Merler S, Cattuto C, Ajelli M. School closure policies at municipality level for mitigating influenza spread: a model-based evaluation. *BMC Infectious Diseases*. 2016;16(1):576. Available from: <https://doi.org/10.1186/s12879-016-1918-z>.
- [33] Colosi E, Bassignana G, Contreras DA, Poirier C, Pierre-Yves B, Cauchemez S, et al. Self-testing and vaccination against COVID-19 to minimize school closure. *Lancet Infect Diseases*. 2022;22:977.
- [34] Gauvin L, Panisson A, Cattuto C. Detecting the community structure and activity patterns of temporal networks: a non-negative tensor factorization approach. *PLoS one*. 2014;9(1):e86028.
- [35] Masuda N, Holme P, editors. *Temporal Network Epidemiology*. Springer, Singapore; 2017.
- [36] Ciaperoni M, Galimberti E, Bonchi F, Cattuto C, Gullo F, Barrat A. Relevance of temporal cores for epidemic spread in temporal networks. *Scientific reports*. 2020;10(1):1-15.
- [37] Pedreschi N, Battaglia D, Barrat A. The temporal rich club phenomenon. *Nat Phys*. 2022;18(8):931-8.
- [38] LaRock T, Lambiotte R. Encapsulation structure and dynamics in hypergraphs. *Journal of Physics: Complexity*. 2023;4(4):045007.
- [39] Barthélemy M, Barrat A, Pastor-Satorras R, Vespignani A. Velocity and hierarchical spread of epidemic outbreaks in scale-free networks. *Physical review letters*. 2004;92(17):178701.
- [40] Candeloro L, Savini L, Conte A. A New Weighted Degree Centrality Measure: The Application in an Animal Disease Epidemic. *PLoS ONE*. 2016 11;11(11):1-14. Available from: <https://doi.org/10.1371/journal.pone.0165781>.
- [41] Dudkina E, Bin M, Breen J, Crisostomi E, Ferraro P, Kirkland S, et al. A comparison of centrality measures and their role in controlling the spread in epidemic networks. *International Journal of Control*. 2023;0(0):1-16.
- [42] Radicchi F, Castellano C. Fundamental difference between superblockers and superspreaders in networks. *Phys Rev E*. 2017 Jan;95:012318. Available from: <https://link.aps.org/doi/10.1103/PhysRevE.95.012318>.
- [43] Chen D, Lü L, Shang MS, Zhang YC, Zhou T. Identifying influential nodes in complex networks. *Physica A: Statistical Mechanics and its Applications*. 2012;391(4):1777-87. Available from: <https://www.sciencedirect.com/science/article/pii/S0378437111007333>.
- [44] Colman E, Holme P, Sayama H, Gershenson C. Efficient sentinel surveillance strategies for preventing epidemics on networks. *PLOS Computational Biology*. 2019 11;15(11):1-19. Available from: <https://doi.org/10.1371/journal.pcbi.1007517>.
- [45] Bucur D, Holme P. Beyond ranking nodes: Predicting epidemic outbreak sizes by network centralities. *PLOS Computational Biology*. 2020 07;16(7):1-20. Available from: <https://doi.org/10.1371/journal.pcbi.1008052>.
- [46] Bajardi P, Barrat A, Savini L, Colizza V. Optimizing surveillance for livestock disease spreading through animal movements. *Journal of The Royal Society Interface*. 2012;9(76):2814-25.
- [47] Valdano E, Poletto C, Giovannini A, Palma D, Savini L, Colizza V. Predicting Epidemic Risk from Past Temporal Contact Data. *PLOS Computational Biology*. 2015 03;11(3):1-19. Available from: <https://doi.org/10.1371/journal.pcbi.1004152>.
- [48] St-Onge G, Iacopini I, Latora V, Barrat A, Petri G, Al-lard A, et al. Influential groups for seeding and sustaining nonlinear contagion in heterogeneous hypergraphs. *Communications Physics*. 2022;5(1):25.
- [49] Stehlé J, Voirin N, Barrat A, Cattuto C, Isella L, Pinton JF, et al. High-resolution measurements of face-to-face contact patterns in a primary school. *PLoS one*. 2011;6(8):e23176.
- [50] Vanhems P, Barrat A, Cattuto C, Pinton JF, Khanafer N, Régis C, et al. Estimating potential infection transmission routes in hospital wards using wearable proximity sensors. *PLoS one*. 2013;8(9).
- [51] Mastrandrea R, Fournet J, Barrat A. Contact patterns in a high school: a comparison between data collected using wearable sensors, contact diaries and friendship surveys. *PLoS one*. 2015;10(9):e0136497.
- [52] Cattuto C, Van den Broeck W, Barrat A, Colizza V, Pinton J, Vespignani A. Dynamics of Person-to-Person Interactions from Distributed RFID Sensor Networks. *PLoS ONE*. 2010 07;5(7):e11596. Available from: <http://dx.doi.org/10.1371/journal.pone.0011596>.

Supplementary material for Infection patterns in simple and complex contagion processes on networks

Diego Andrés Contreras, Giulia Cencetti, Alain Barrat

Section S1. INFECTION PATTERN ASYMMETRY AND SIMILARITY WITH ADJACENCY MATRIX

We report in Fig. S1 the similarity of the infection patterns with the weighted adjacency matrix (left panels) for the simple, simplicial, and threshold models, as a function of the model parameters. The similarity is high but less than 1, and lower for the simplicial and especially the threshold model. We also observe that similarity slightly decreases when increasing R_0 for the model of simple spread and when decreasing θ in threshold model, i.e. when increasing the infection probability on each link. In extreme cases, indeed, the infection probabilities saturate and contagions are possible on each existing link independently on its weight. Smoothing out the differences between weights implies reducing the similarity of the infection patterns with the adjacency matrix. In the simplicial model instead the similarity with the adjacency matrix decreases when increasing β_Δ/β_1 , i.e. when infection events are favored on triangular interactions with respect to link interactions.

The right panels of Fig. S1 report the distributions of the symmetry of the contact patterns, as quantified by the ratio between link weights in opposite directions of each pair of connected nodes, for the three models of contagion. Specifically, for each edge (i, j) we report the infection probability in the direction that has been less used divided by the infection probability in the opposite direction, $\min(C_{ij}, C_{ji})/\max(C_{ij}, C_{ji})$. For symmetric infection patterns, this quantity is 1 for each edge, and 0 in the extreme case of an edge in which the contagion is observed only in one of the two possible directions.

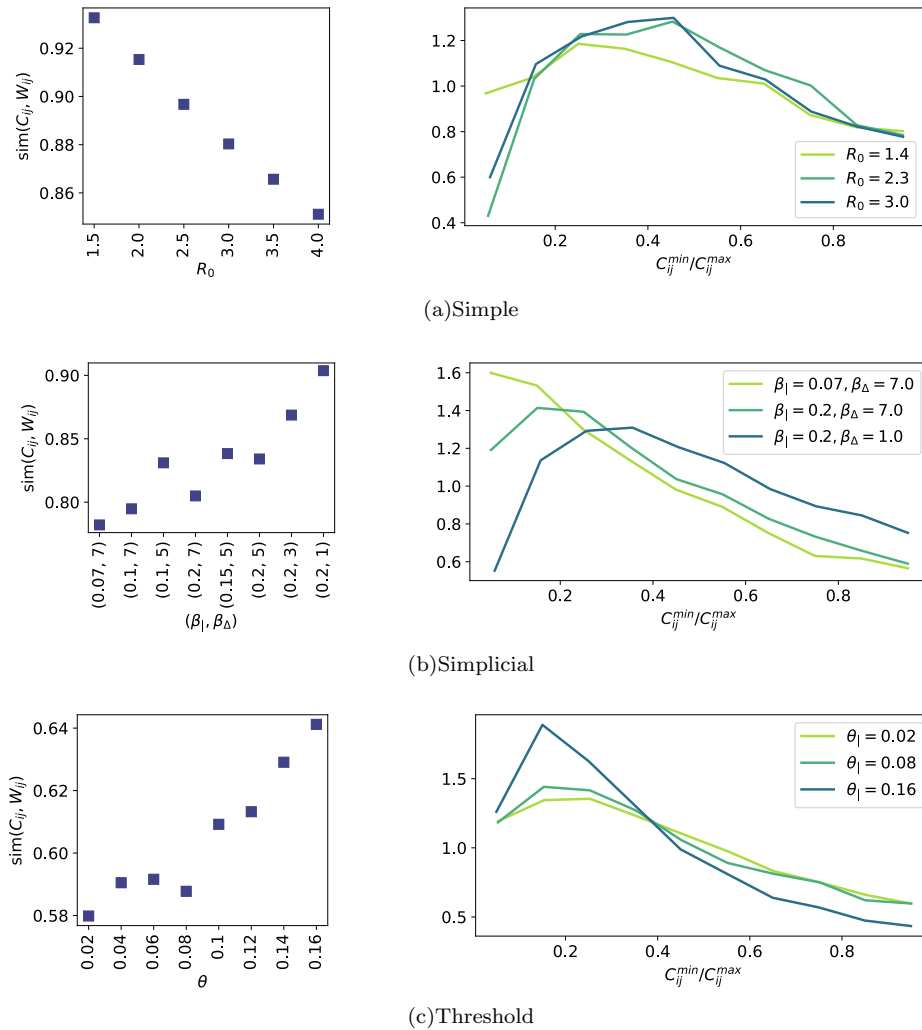


FIG. S1. Cosine similarity between infection pattern \mathbf{C} and weighted adjacency matrix \mathbf{W} on the left, and distribution of symmetry in infection pattern on the right.

Section S2. EPIDEMIC CURVES IN SIMPLE CONTAGION

Figure S2 shows the temporal evolution of the number of infected in various models of simple contagion. These involve only infected for the SIR model, and exposed and infected for the other models. The time evolution of the epidemic is clearly different across models.

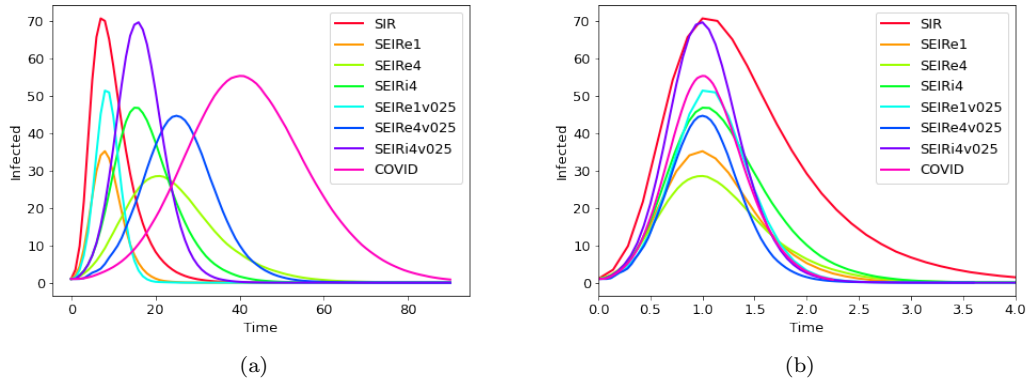


FIG. S2. Number of infected individuals vs. time for different models of simple contagion (I for SIR model, E+I for all the SEIR models), with $R_0 = 3.0$. In the right panel the time has been normalized so as to have the maximum peak at $t = 1$ for all models.

Section S3. WEIGHTED ADJACENCY IN NETWORKS AND IN SIMPLICIAL COMPLEXES

In the main text we mentioned that for real networks higher-order and pairwise interactions largely overlap, i.e., nodes connected in groups with large weights are typically also connected by links with large weights. To show this we report in Fig. S3 a scatterplot where for each pair of nodes (i, j) we show the pairwise weight W_{ij} and the second-order weight of all the triads that the pair is involved in, $\sum_k W_{ijk}^\Delta$, for the five different data sets. The Pearson correlation is reported in each panel.

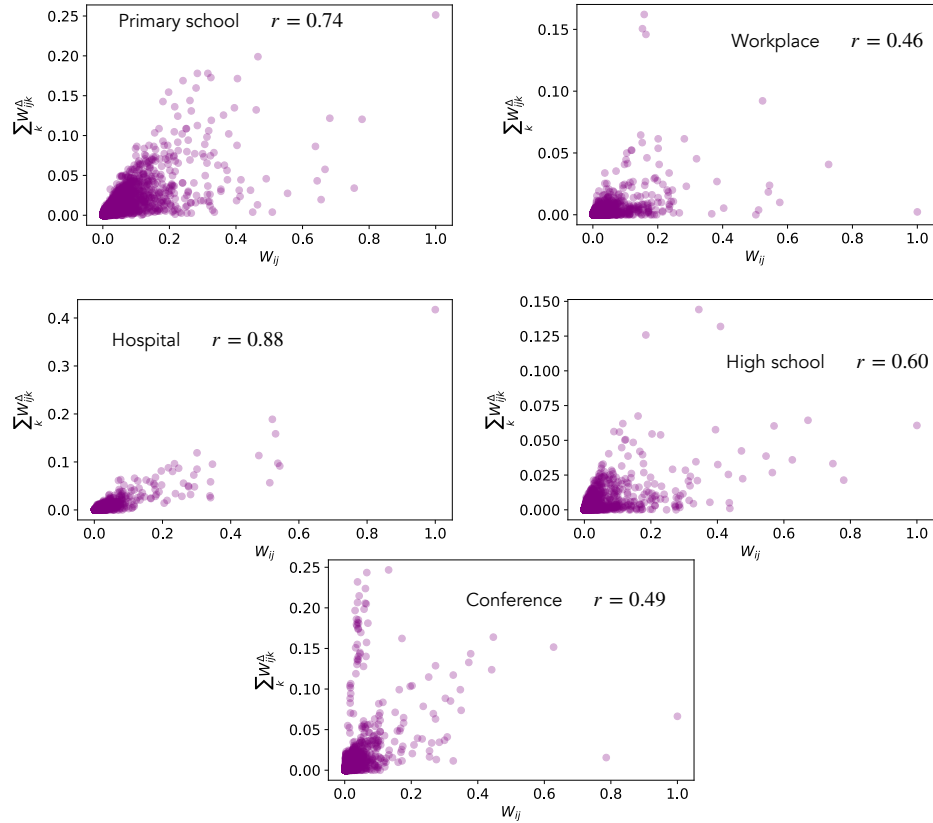


FIG. S3. Correlation between link weight and triads weights for each couple of nodes in each network.

Section S4. UNCORRELATED HYPERGRAPHS

As mentioned in the main text and illustrated in the previous section, the hypergraphs built from real data sets present a high correlation between the weights of first and second order interactions: if a hyperedge (i, j, k) has a high (low) weight we typically observe that the pairwise interactions (i, j) , (j, k) and (k, i) are also associated to high (low) weights. This can explain the high values of similarity that we observed in section II C between infection patterns obtained at varying parameters (β, β_Δ) . Indeed, changing such parameters leads to a shift from having more contagion events through links than in triadic interactions (for high β , low β_Δ) to the reverse situation (at low β and high β_Δ). However, the fact that the weights of links and triadic interactions are correlated means that this shift does not lead to strongly different infection patterns.

To better show this point, we perform here an additional set of numerical experiments. We first build synthetic hypergraphs in which we remove the correlations between the weights of the links and of the triads. To this aim, we consider the original hypergraph, keep its structure fixed (list of links and triads), keep as well the weights of the triads fixed, but reshuffle the weights of the links. Note that we still have a correlation between the first and second order interactions as those largely overlap in the data. However, one can have a triad with a large weight composed of links with small weights and vice-versa, with overall no weight correlations. This absence of correlations is checked in Fig. S4(f) which, analogously to Fig. S3, is a scatterplot reporting for each link its weight and the sum of weights of all triads involving that link: we obtain a very small coefficient correlation (here for the primary school data set), while it was of 0.74 in the original data (see Fig. S3). We then simulated the simplicial contagion process on the hypergraph with no weight correlations, measured the infection patterns for the same parameter values as in the main text, and performed the same comparisons between the patterns obtained for different parameters.

Figure S4 reports the corresponding results for the primary school data set, in a way analogous to Fig. 5 of the main text. Note that, to obtain panel (e), we simulate the simple contagion process using the same link weights as in the reshuffled hypergraph. The similarity values we obtain are notably lower than in the original hypergraph, confirming that the high similarity observed in the real hypergraphs is largely due to the correlations between the weights of the first and second order interactions.

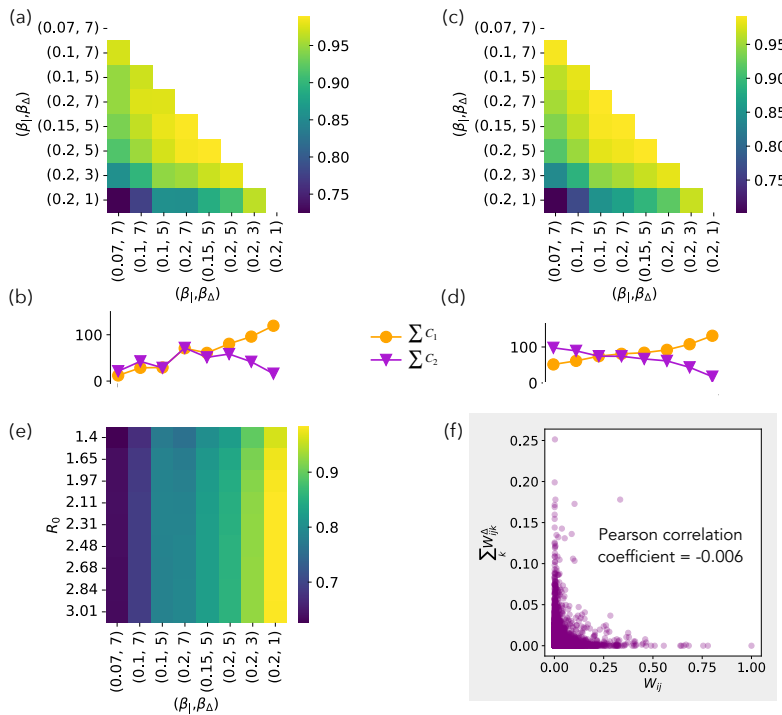


FIG. S4. Infection patterns for simplicial contagion models simulated on the hypergraph obtained from the primary school data set and with reshuffled weight links. Panels (a) to (e) are built similarly to the ones of Fig. 5 of the main text. (a): Cosine similarity between infection patterns obtained with different combinations of β_1 and β_Δ . (b): Number of contagions taking place via first and second order hyperedges in the simulations of the previous panel. (c): Same as (a) but when the infection patterns are computed using only simulations with attack rate between 0.6 and 0.7. (d): Number of contagions taking place via first and second order simplices in the simulations of the previous panel. (e): Cosine similarity between the infection patterns of the simplicial contagion model (for the same range of values of β_1 and β_Δ) and simple contagion (for several values of R_0). (f): Correlation between link weight and triads weights for each couple of nodes in the hypergraph with reshuffled link weights, similarly to Fig. S3.

Section S5. DISTRIBUTIONS OF FINAL ATTACK RATES IN THE SIR SIMPLE CONTAGION MODEL

In simple contagion processes, the final attack rate (number of nodes that have been infected at the end of the process) depends on the stochastic realizations, even at fixed parameters. To each value of R_0 , we can thus associate a distribution of final attack rate values, which we build by collecting the final attack rates of all the numerical simulations with the same R_0 . Figure S5 shows the obtained distributions for the SIR model and different choices of R_0 , built with 1000 stochastic runs for each R_0 . In particular, panel (a) shows the attack rate for the values of R_0 used in Fig. 3(c) of the main text. On the right we report for each R_0 the percentage of these simulations that yield a final attack rate between 0.75 and 0.85. For instance, only about 3% of runs fall into this interval for $R_0 = 1.65$. Panel (b) analogously shows the attack rate for the lower values of R_0 used in Fig. 3(d-e) and, on the right, the percentage of simulations that fall into the intervals (0,0.2) and (0.5,0.6).

The infection patterns used in Fig. 3(c) are the result of the average over 1000 simulations for each R_0 , which means that we actually perform a much larger number of simulations, in fact as many as needed until we have obtained 1000 simulations with final attack rate in the desired range. For instance, for $R_0 = 1.65$ we need around 33000 simulations. The infection patterns used in Fig. 3 (d) and (e) are instead averaged over 10000 and 50000 runs, respectively. So for instance with $R_0 = 1.72$, in order to find enough instances with attack rate between 0.5 and 0.6 we need around 200000 simulations.

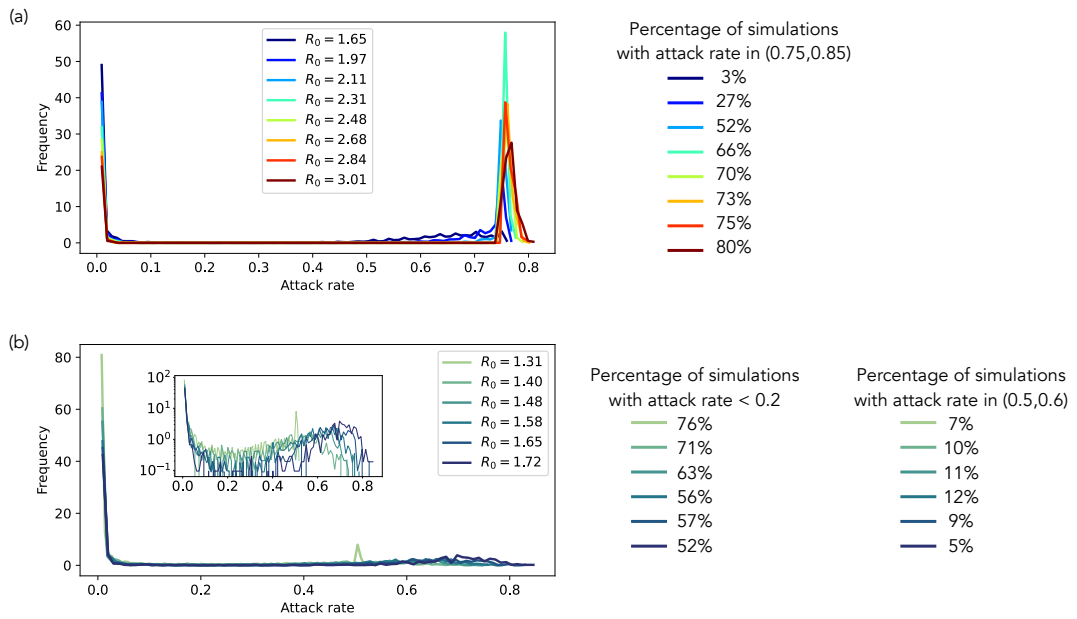


FIG. S5. Distributions of final attack rates in numerical simulations of SIR simple contagion processes for different values of R_0 , for the primary school data set. Each distribution is obtained from 1000 numerical simulations with random initial conditions. In panel (b) the inset shows the same distributions with a logarithmic y scale.

Section S6. SPREADER AND RECEIVER INDICES

Starting from the infection pattern matrix \mathcal{C} we can define two indicators that characterize the role of each node by quantifying their ability to spread and to receive:

- **Spreader index** $s_i = \sum_j C_{ij}$: expected number of direct infections produced by node i .
- **Receiver index** $r_i = \sum_j C_{ji}$: expected number of direct infections received by node i .

We report the two indices for simple, simplicial, and threshold contagion in Figs. S7, S8, S6, S9, S10 and S11, showing the relation between s_i and r_i , and the similarity (cosine and ranking) of each of them at varying parameters. We notice that these measures, even if they are correlated among them, do not coincide. This is due to the asymmetry of matrix \mathbf{C} and implies that having a large probability of being infected does not necessarily correspond to a large spreading ability, as it has been recently discussed in literature [42].

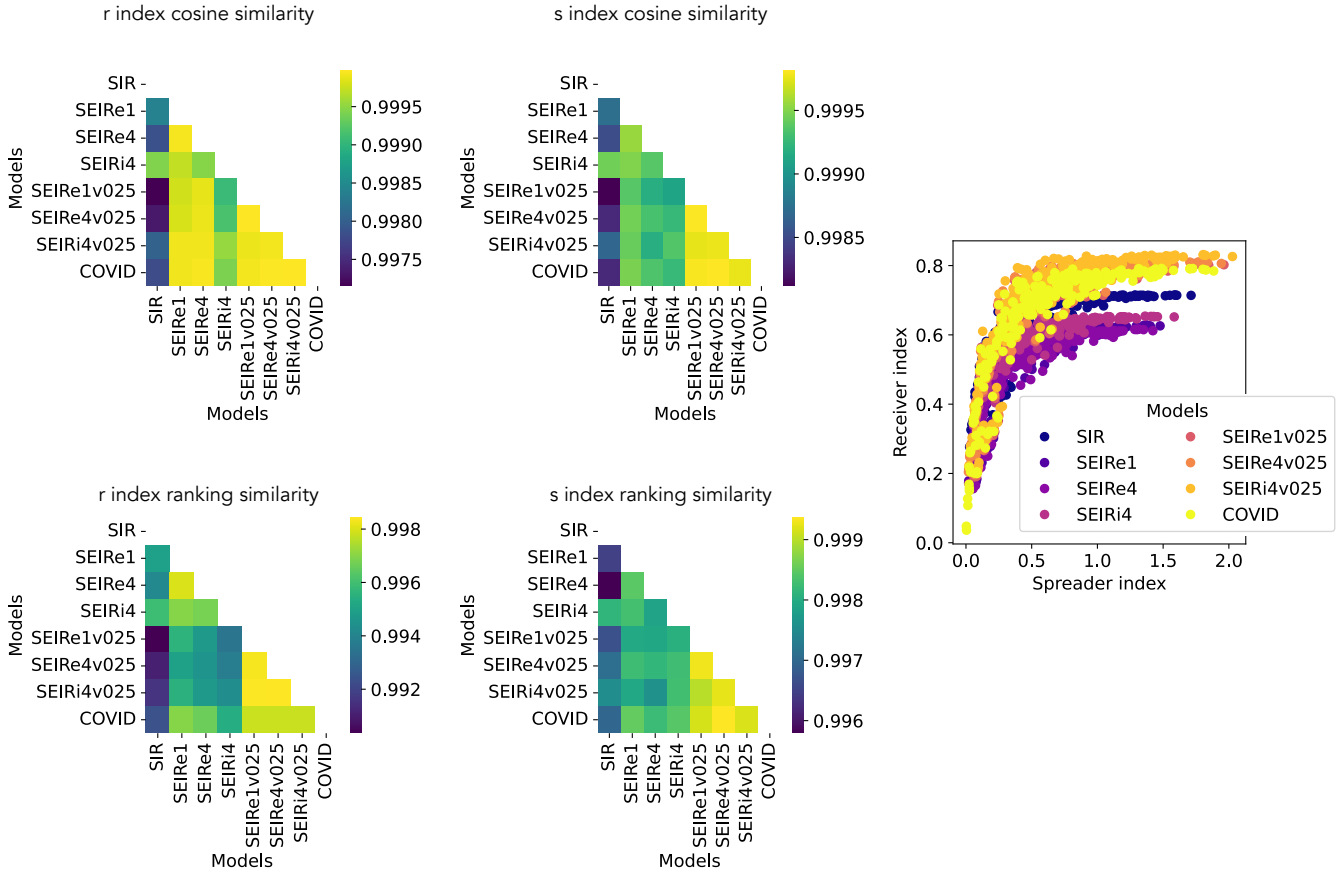


FIG. S6. Receiver and spreader indices across models of simple contagion with fixed $R_0 = 2.5$ for the primary school data set.

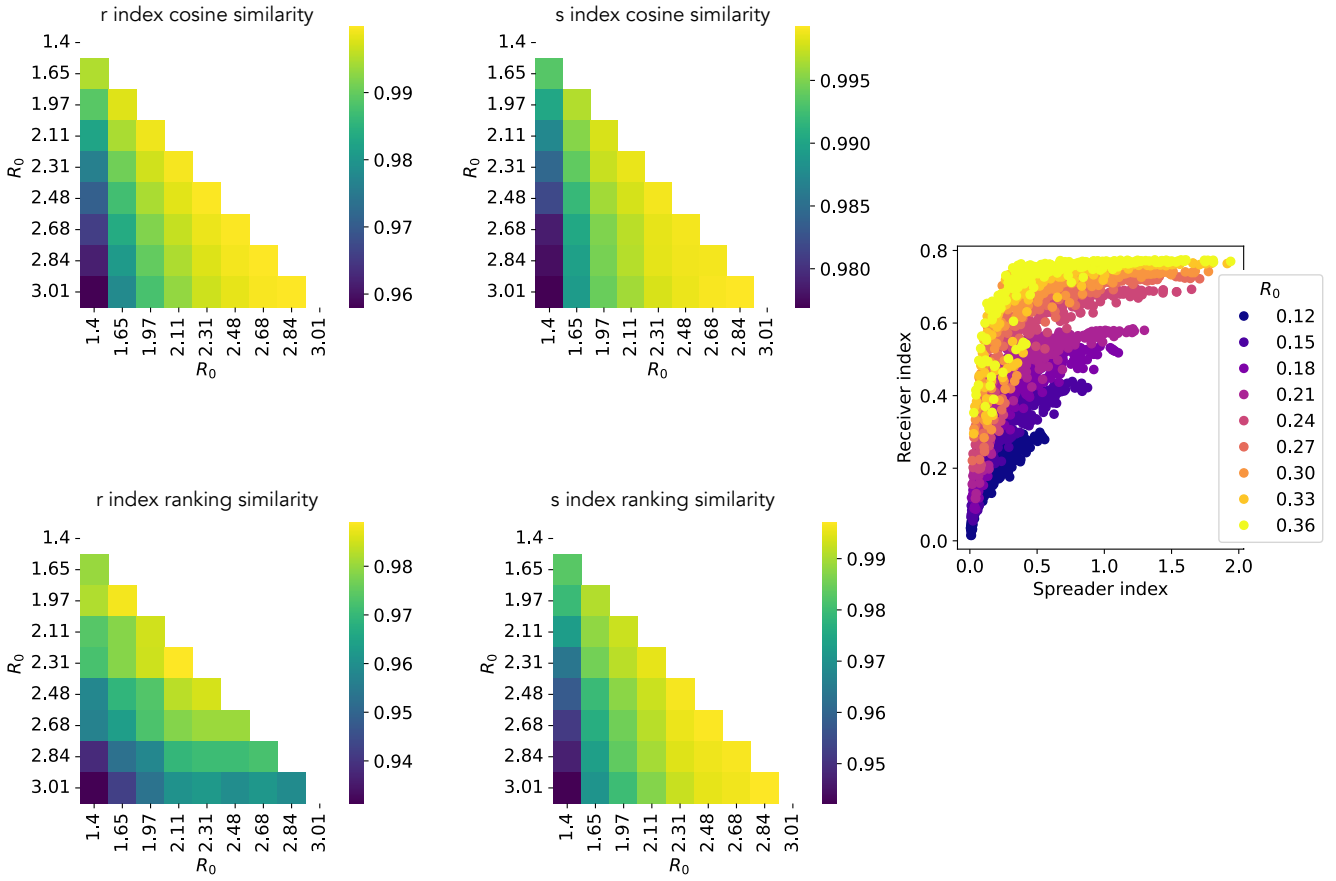


FIG. S7. Receiver and spreader indices across values of R_0 in simple contagion (SIR model) for the primary school data set.

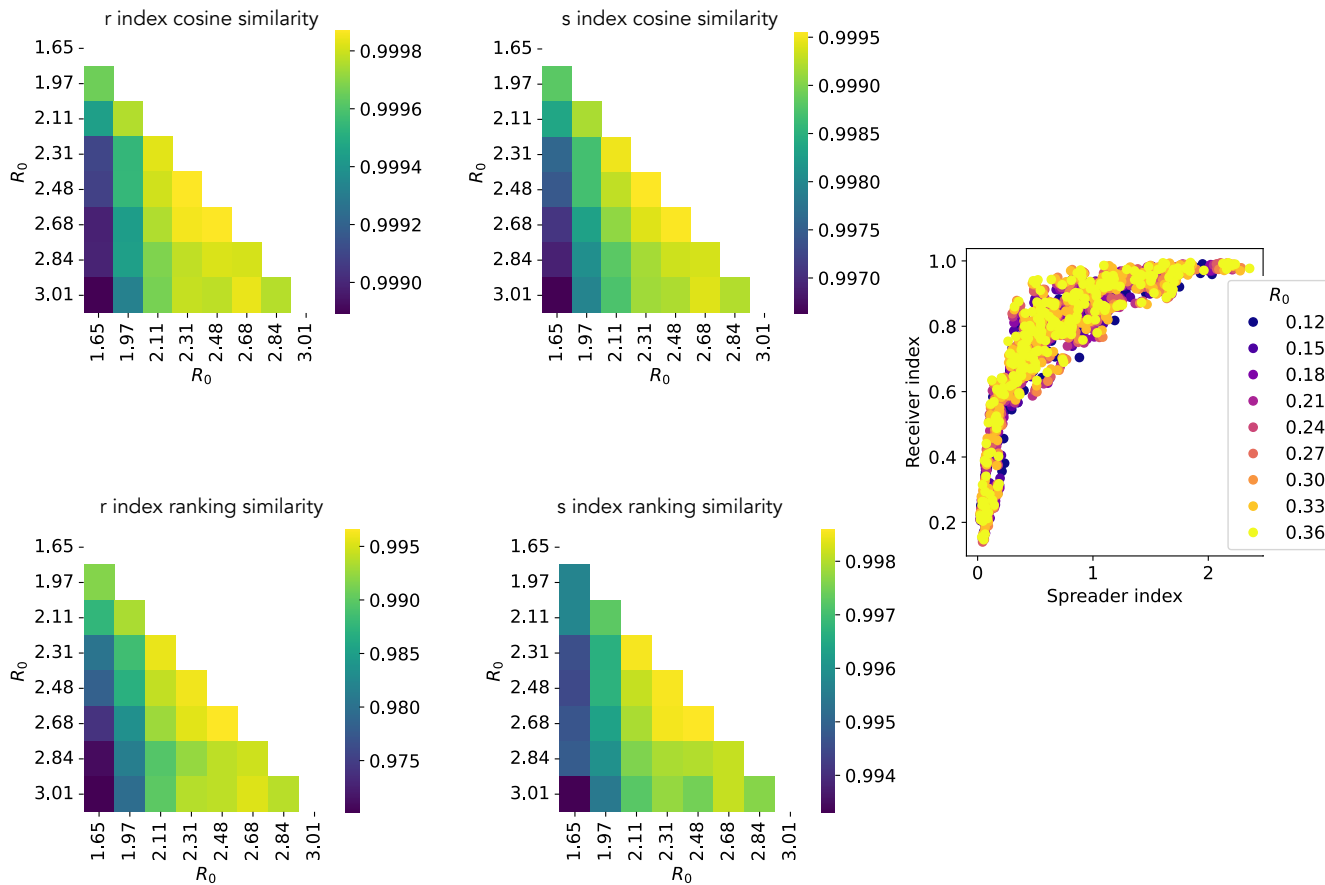


FIG. S8. Receiver and spreader indices across values of R_0 in simple contagion (SIR model) with fixed attack rate $0.75 < a < 0.85$ for the primary school data set.

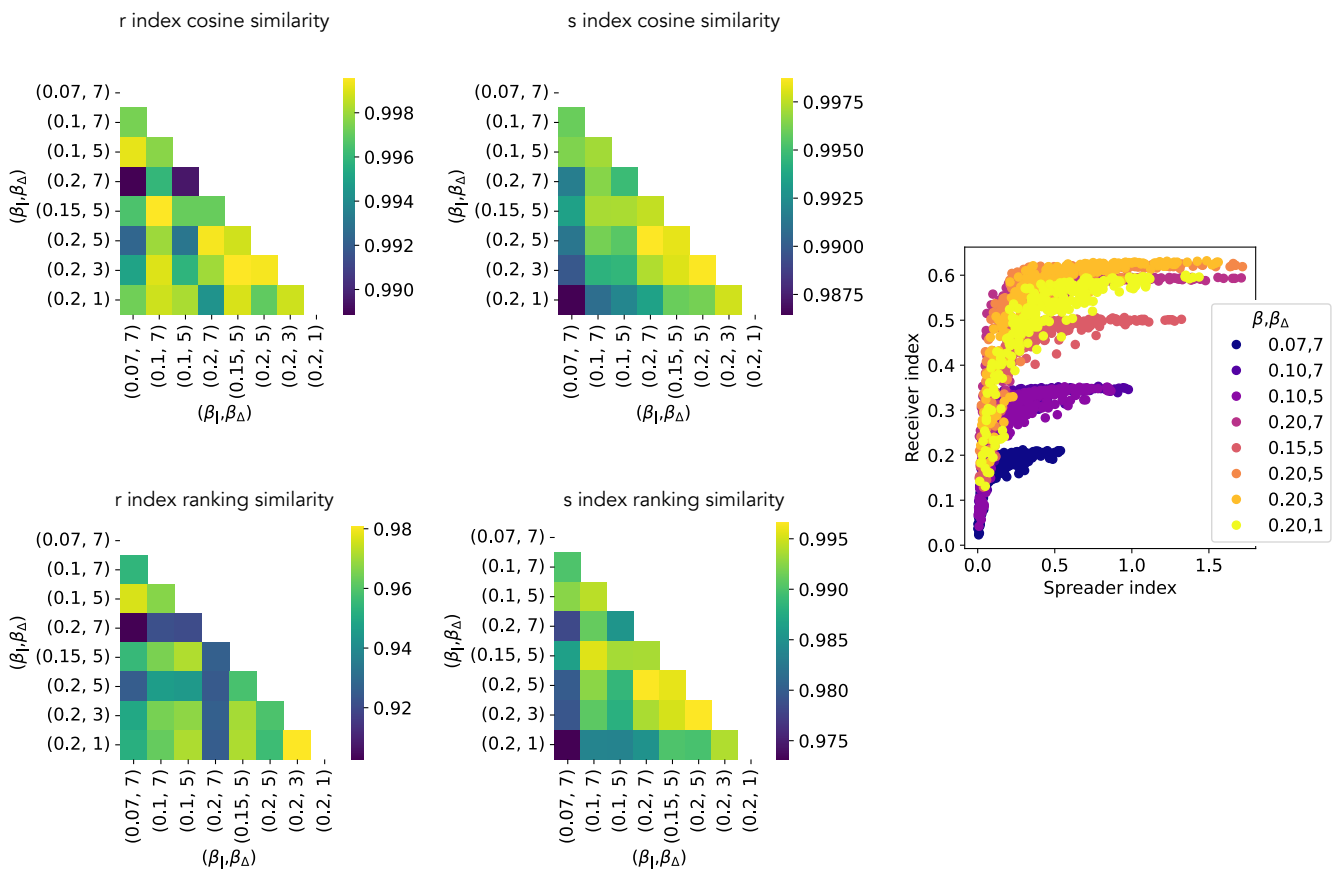


FIG. S9. Receiver and spreader indices in simplicial contagion for the primary school data set.

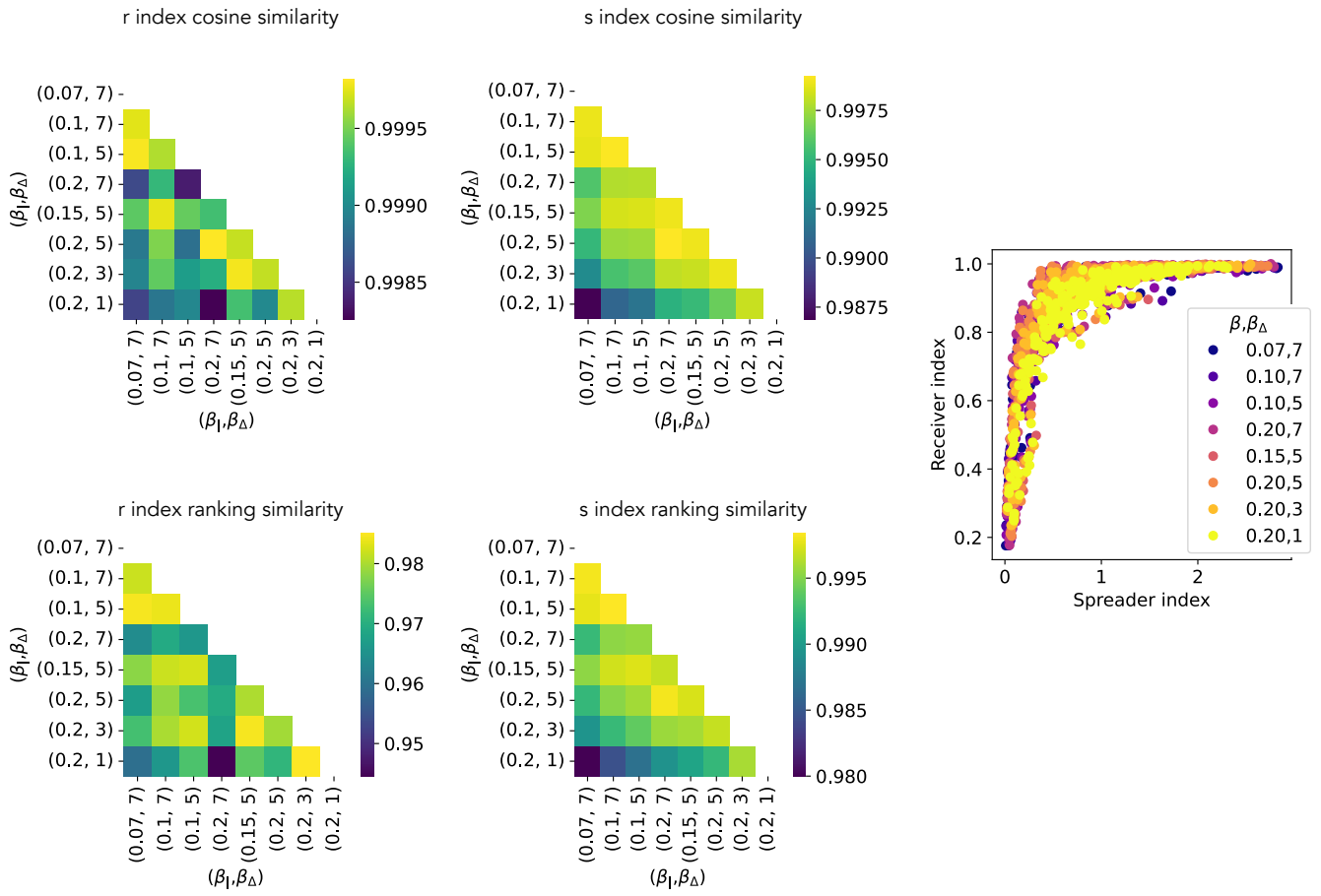


FIG. S10. Receiver and spreader indices in simplicial contagion with fixed attack rate $0.8 < a < 0.9$ for the primary school data set.

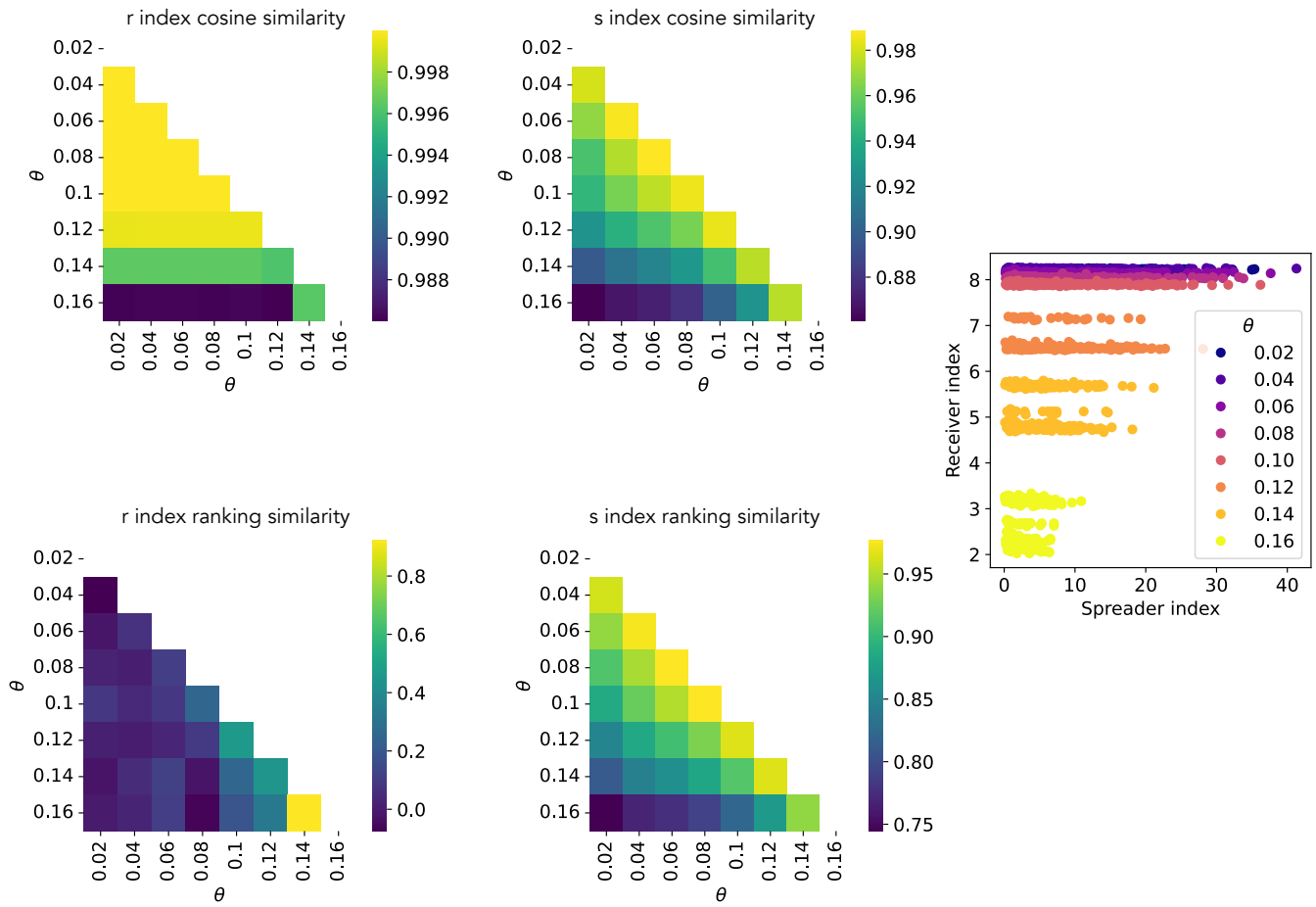


FIG. S11. Receiver and spreader indices in threshold contagion for the primary school data set. The low values of the ranking similarity for the r index are due to the fact that r spans a very narrow interval of values for each θ (see scatterplot), i.e., there is very little heterogeneity in the indices of different nodes.

Section S7. RESULTS FOR OTHER DATA SETS

In the following figures we report the results on infection pattern similarity (for the different models of contagion and across models) for simulations performed on four additional networks of face-to-face interactions, measured in a conference [27], a hospital [28], a workplace [27] and a high school [30]. The results are in line with those of the primary school contact network presented in the main text.

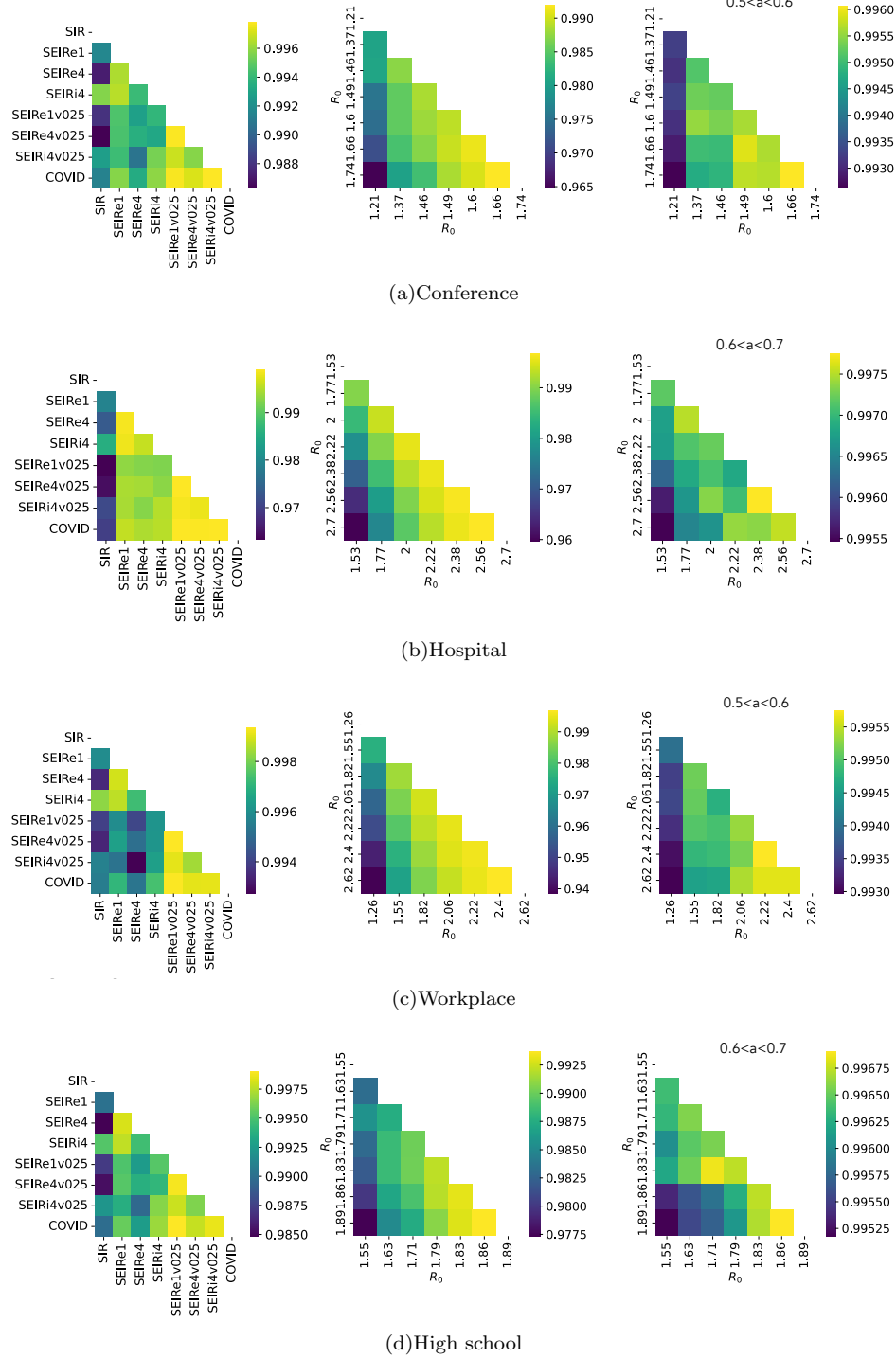
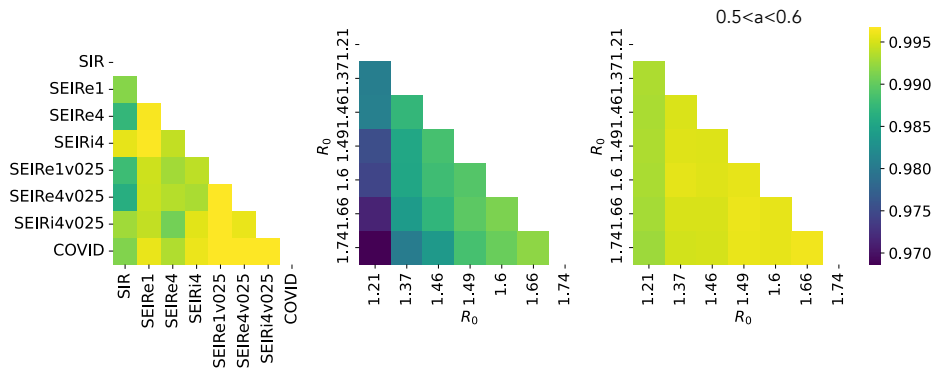
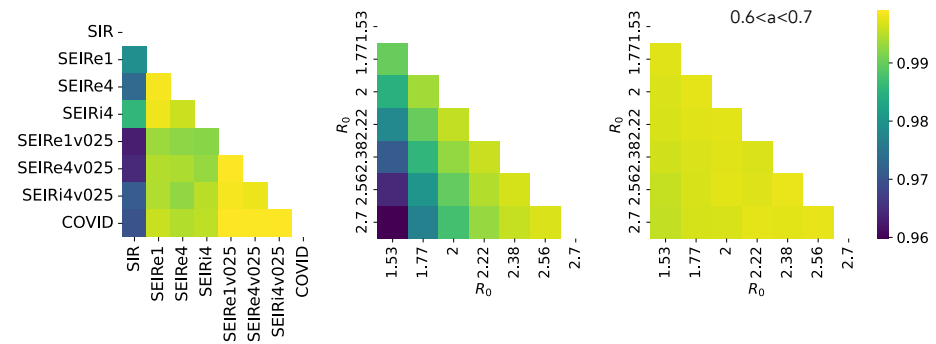


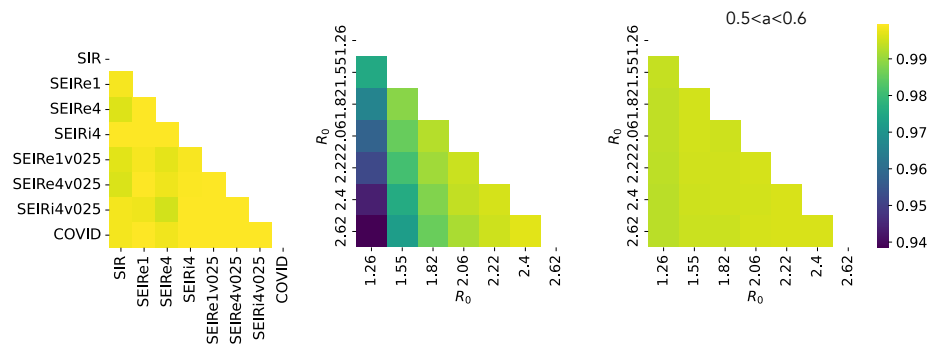
FIG. S12. Infection patterns in simple contagion. For each data set, the panel on the left reports the infection pattern similarity between different models of simple contagion (with $R_0 = 2.5$), the central panel the similarity between patterns obtained at different values of R_0 (with the SIR model), and the panel on the right shows the same but at fixed attack rate.



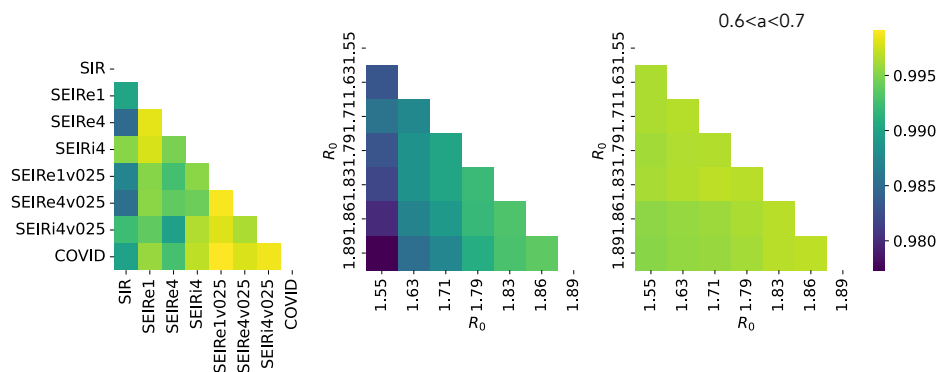
(a)Conference



(b)Hospital



(c)Workplace



(d)High school

FIG. S13. Same as Fig. S12 with the same colorscale in all panels of a given data set.

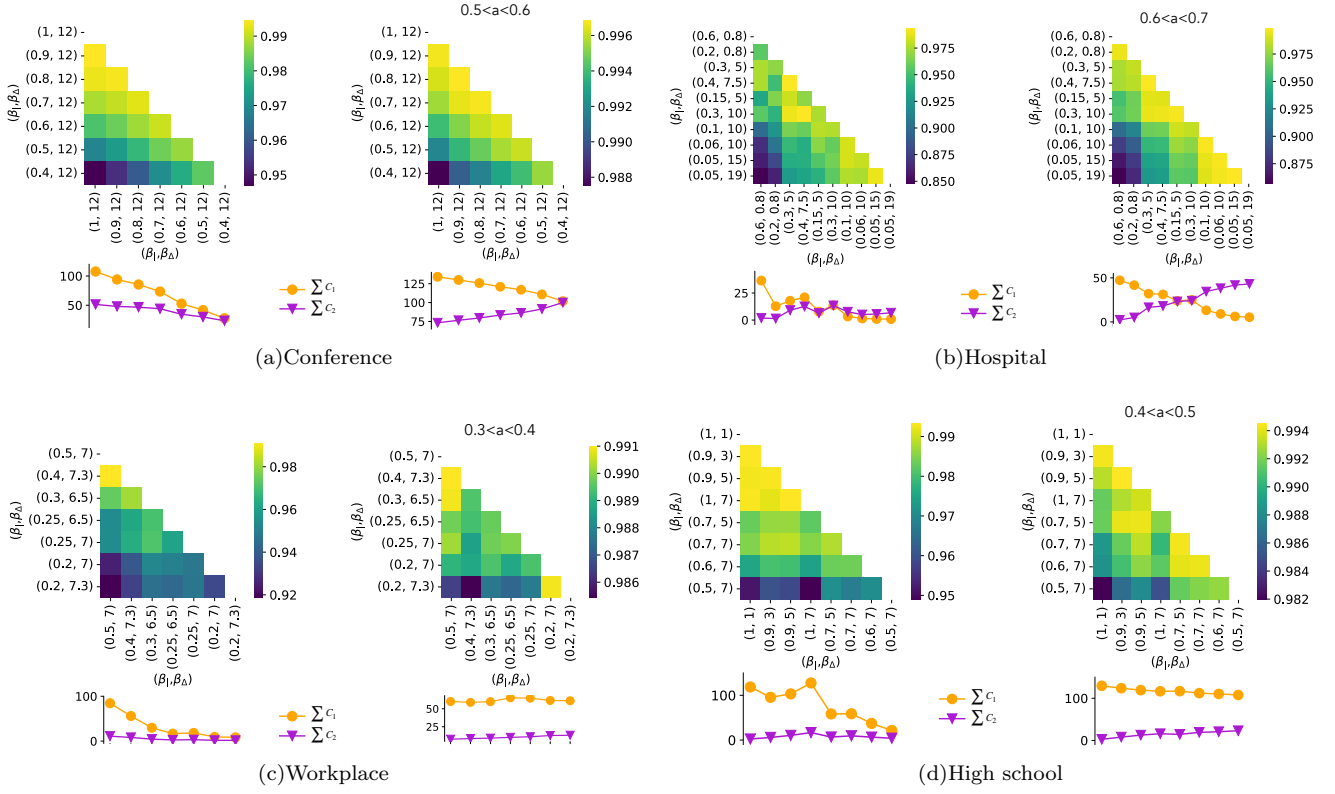


FIG. S14. Infection patterns in simplicial contagion. For each data set, the panel on the upper left reports the infection pattern similarity for different values of β_1 and β_{Δ} , just below the number of contagions taking place via first and second order simplices is depicted. The panels on the right show the infection pattern similarity and numbers of first and second order interactions when the attack rate is fixed.

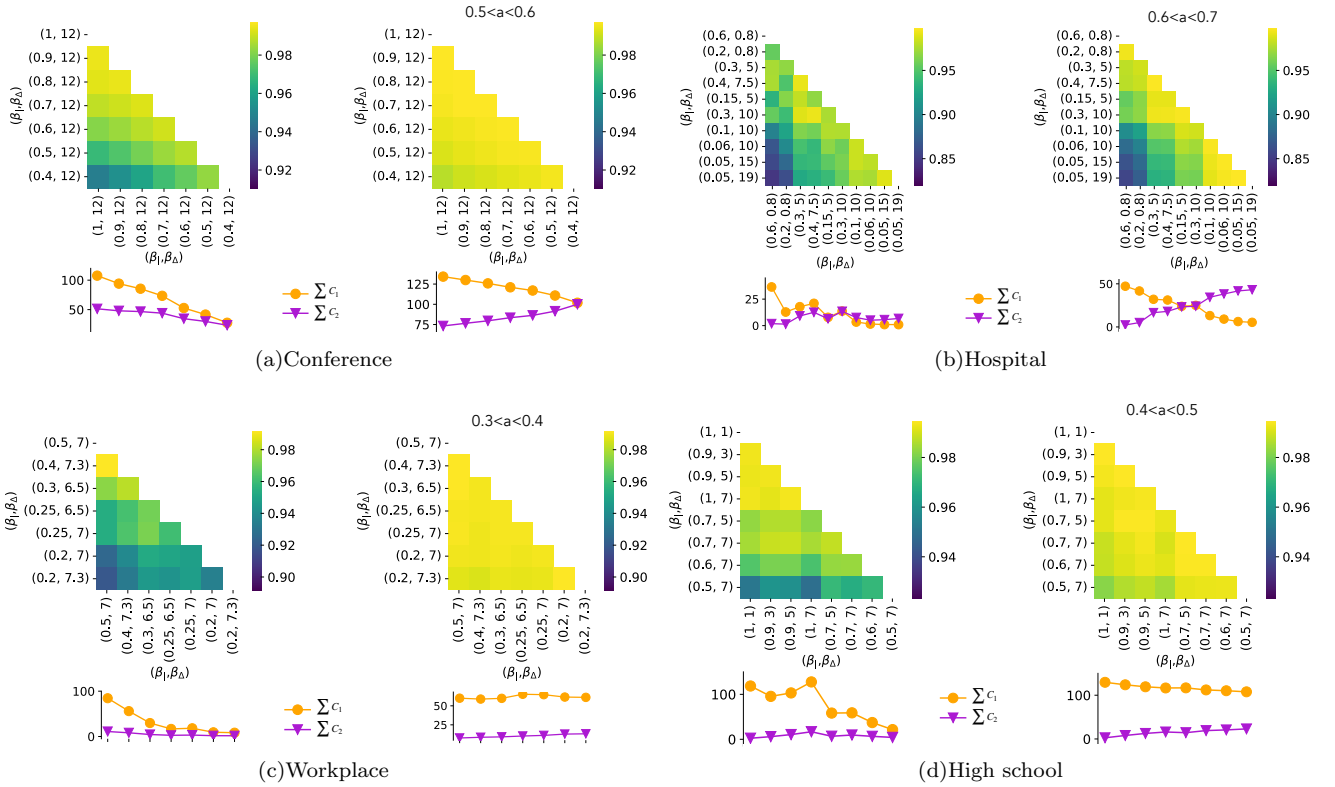


FIG. S15. Same as Fig. S14 with the same colorscale in all panels of a given data set.

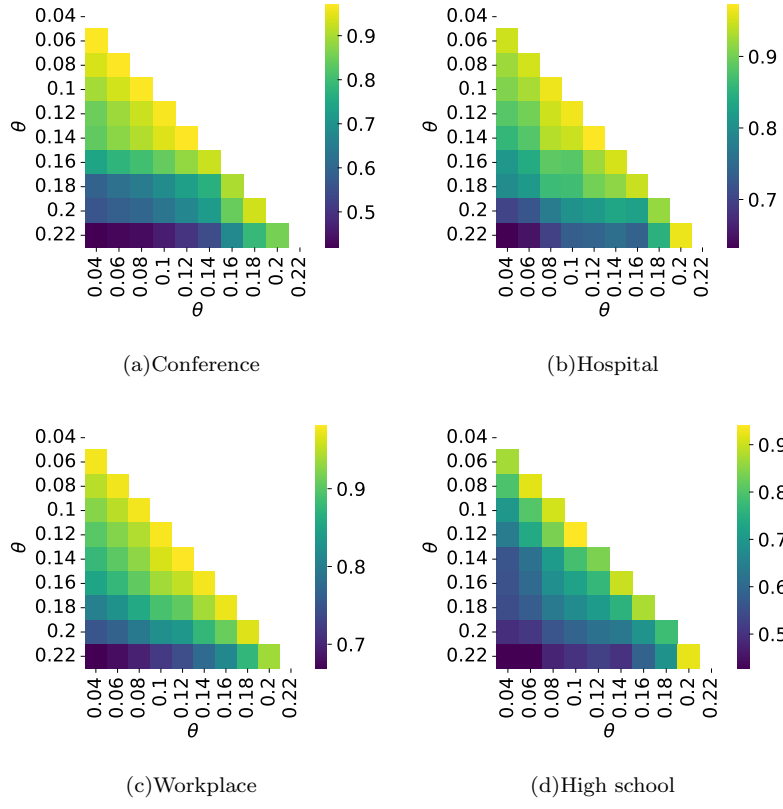


FIG. S16. Infection patterns in threshold contagion: similarity between the patterns obtained with different values of θ and for different data sets.